AD NUMBER

AD603342

LIMITATION CHANGES

TO:

Approved for public release; distribution is unlimited.

FROM:

**Distribution authorized to U.S. Gov't. agencies and their contractors;
Administrative/Operational Use; AUG 1964. Other requests shall be referred to Air Force Arnold Engineering Development Center, Arnold AFB, TN.**

AUTHORITY

dtic form 55

AEDC-TDR-64-107

UNCLASSIFIED

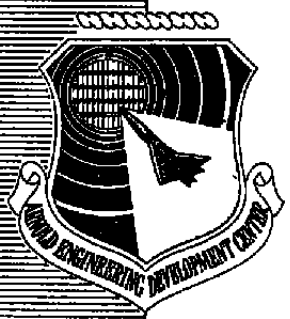

STUDY OF ELECTRODE ATTACHMENT REGIONS IN HIGH CURRENT GASEOUS DISCHARGES

By

Dr. Gordon L. Cann

Electro-Optical Systems, Inc.
Pasadena, California

TECHNICAL DOCUMENTARY REPORT NO. AEDC-TDR-64-107

August 1964

Program Element 61405014/8951, Task 895101

(Prepared under Contract No. AF 40(600)-987 by Electro-Optical Systems, Inc., Pasadena, California.)

ARNOLD ENGINEERING DEVELOPMENT CENTER

AIR FORCE SYSTEMS COMMAND

UNITED STATES AIR FORCE

Unclassified

NOTICES

Qualified requesters may obtain copies of this report from DDC, Cameron Station, Alexandria, Va. Orders will be expedited if placed through the librarian or other staff member designated to request and receive documents from DDC.

When Government drawings, specifications or other data are used for any purpose other than in connection with a definitely related Government procurement operation, the United States Government thereby incurs no responsibility nor any obligation whatsoever; and the fact that the Government may have formulated, furnished, or in any way supplied the said drawings, specifications, or other data, is not to be regarded by implication or otherwise as in any manner licensing the holder or any other person or corporation, or conveying any rights or permission to manufacture, use, or sell any patented invention that may in any way be related thereto.

STUDY OF ELECTRODE ATTACHMENT REGIONS IN HIGH CURRENT GASEOUS DISCHARGES

By
Dr. Gordon L. Cann
Electro-Optical Systems, Inc.
Pasadena, California

(The reproducibles used in the reproduction of this report were supplied by the authors.)

August 1964

FOREWORD

This report was prepared by Dr. Gordon L. Cann and Mr. Robert L. Harder of the Fluid Physics Division of Electro-Optical Systems, Inc., under USAF Contract No. AF 40(600)-987. The report covers research conducted from 18 June 1962 through 18 September 1963.

ABSTRACT

This report discusses an experimental and theoretical study of electrode attachment regions in a high-current gaseous discharge, particularly in the mechanisms causing retrograde motion of the arc attachment spot on the cathode. Work included mathematical analysis and formulation of a theory of cathode emission under these operating conditions and experimental investigations to correlate the theory with observed effects.

Experiments and apparatus for measuring power loss to arc cathodes were set up. Analysis of the retrograde motion of the cathode spot was made, and experiments to confirm the analysis were performed.

The study has resulted in the definition of a mathematical problem. The MHD equations must be solved in the electrode and in the gas, and the two solutions matched at the interface.

PUBLICATION REVIEW

This report has been reviewed and publication is approved.

Larry D. Fitzgerald
Capt, USAF
Aerospace Sciences Division
DCS/Research

Donald R. Eastman, Jr.
DCS/Research

TABLE OF CONTENTS

		Page
1.	INTRODUCTION	1
2.	ELECTRODE ATTACHMENT REGIONS IN HIGH CURRENT DISCHARGES	2
	2.1 Statement of the Problem	2
	2.2 Mathematical Formulation of the Problem	5
3.	ENERGY BALANCE	12
	3.1 Energy Balance in the Metal	12
	3.2 Heat Balance in an Arc Near the Attachment Point	21
	3.3 Heat Balance at the Cathode Surface	26
	3.4 Heat Balance at the Anode Surface	31
4.	CATHODE SPOT EXPERIMENT	34
	4.1 Test Geometry	34
	4.2 Instrumentation	39
	4.3 Experimental Results	39
5.	RETROGRADE MOTION OF THE CATHODE SPOT	43
	5.1 Analysis of Retrograde Effect	43
	5.2 Retrograde Motion Experiment	48
6.	CONCLUSIONS	56
7.	RECOMMENDATIONS	57
	REFERENCES	58

LIST OF FIGURES

		Page
1	Postulated Cathode Mechanisms	6
2	Model Used for Solving the Energy Equation in the Electrode	13
3	Thermal Conductivity Integral vs Temperature for Tungsten (Determined from Data of Ref. 4)	15
4	Thermal Conductivity Integral vs Temperature for Copper (Determined from Data of Ref. 4)	16
5	Electrical Resistivity of Tungsten vs ϕ (Determined from Data of Ref. 4)	17
6	Electrical Resistivity of Copper vs ϕ (Determined from Data of Ref. 4)	18
7	Model Used for Solving the Energy Equation in the Gas	22
8	Dimensionless Conductivity Integral in Arc vs Distance from Cathode Surface	25
9	Vapor Pressure and Thermionic Emission Current Density for Tungsten (Determined from Data of Ref. 5)	29
10	Vapor Pressure and Thermionic Emission Current Density for Copper (Determined from Data of Ref. 5)	30
11	Theoretical Solutions for Tungsten Cathode	32
12	Theoretical Solutions for Thoriated Tungsten Cathode	33
13	Schematic Drawing of Cathode Test Apparatus	35
14	Early Arc Cathode Assembly	36
15	Components for Arc Cathode Study	37
16	Assembled Equipment for Cathode Study	38
17	Cathode Attachment and Column During Operation	40
18	Comparison of Measured and Theoretical Values for Cathode Power	41
19	Retrograde Motion Experimental Apparatus	50
20	Retrograde Motion Apparatus Magnetic Circuit Components (Disassembled)	51
21	Retrograde Motion Apparatus Magnetic Circuit Components (Assembled)	51
22	Magnetic Circuit Retrograde Motion Apparatus - Phase I	53
Table I	Instruments Used in Cathode Spot Experiment	42

LIST OF SYMBOLS

A	Cross-section Area
B	Magnetic Field
c	Constant Defined by Equation (64)
D	Particle Diffusion Coefficient
E	Electric Field
$\|e\|$	Charge of an Electron
F_1	Defined in Equation (57)
F_1'	F_1 - VxB
F_2	Defined in Equation (58)
f	Correction Term in Diffusion Coefficient
h	Planck's Constant
I	Total Current
J	Charged Particle Flux
$J_o(),J_1()$	Bessel Functions
$\mathcal{J}$	Defined in Equation (63)
j	Current Density
K	Thermal Diffusion Coefficient
k	Boltzmann Constant
L_1	Defined in Equation (62)
M	Defined in Equation (61)
m_e	Mass of Electron
n	Number Density
P	Power
P	Pressure
p_r	Radiated Power per Unit Volume
p	Pressure
Q	Defined in Equation (65)

q	Heat Flux
$(q_o)_{metal}$	Surface Heat Flux
q	Collision Cross-section
r	Polar Radial Coordinate in Electrode, Origin at Apex of Cone
r	Cylindrical Coordinate in Arc, Origin Along Centerline
r_o	Polar radial coordinate of Electrode Surface (See Fig. 2)
r'	Constant Defined by Equation (19)
s	Dimensionless Coordinate Defined in Equation (34)
T	Temperature
T_e	Electron Temperature
T_s	Surface Temperature
U	Absolute Velocity of Ions and Electrons Moving Together
U	Dummy variable at Integration in Equation (37)
u	Velocity
V	Volume
v	Velocity
x	Direction of Motion of Cathode Spot
y	Direction of Electric Discharge
z_I	Ionization Number
z	Axial Coordinate of Arc, Origin at Electrode Surface
z	Direction of Applied Field
β_1	Defined in Equation (59)
ϵ_o	Capacitivity of Vacuum
θ	Semi-apex Angle of Conical Electrode (See Fig. 2)
κ	Thermal Conductivity
λ	Distance from Surface to Critical Plane
μ_o	Permeability of Vacuum
μ_e	Electron Chemical Potential
ρ	Electrical Resistivity

σ	Electrical Conductivity
τ_e	Collision Time for Electrons
τ_I	Collision Time for Ions
Φ	Conductivity Integral (See Equation 17)
$(\xi_o)_{metal}$	Surface Temperature of Electrode Tip
Φ_1, Φ_2	Arbitrary Constants of Integration
ϕ	Conductivity Integral (See Equation 15)
ϕ_{gas}	Value of ϕ of the gas at the Electrode Attachment
χ	Work Function
ω_e	Gyration Frequency of Electrons
ω_I	Gyration Frequency of Ions

1. INTRODUCTION

Electrode phenomena in high current electric discharges have been studied extensively ever since arcs were discovered. A vast body of literature on the subject has accumulated. It is summarized and referenced in Ref. 1 of this report. Despite the considerable effort that has been expended, little or no engineering information is available to the designer of arc devices. Such fundamental questions as the anode and cathode configuration and material, the material loss rate from the electrodes, or the power loss rate to the electrodes must be determined empirically, if at all. Even more important, the attachment area of the discharge to the electrode cannot be predicted. Since some devices require specific attachment configurations in order to operate, the design can easily fail due to a lack of knowledge of how to design for the required electrode configuration. In many cases, it is probable that a true understanding of electrode attachment phenomena would show the infeasibility of many gas discharge and magnetogasdynamic (MGD) devices which, if assessed only on the basis of volume effects in the gas discharge, would seem promising.

In the past, a great deal of attention has been paid to examining special mechanisms that may be operating in the electrode attachment regions. In this report, an effort will be made to incorporate all of these into simple analytic expressions that describe the gross properties of the zones only. Although the various processes cannot now be described exactly, it is hoped that the simplicity gained can help in obtaining phenomenological understanding of the attachment region and eventually lead to the development of electrode design criteria.

2. ELECTRODE ATTACHMENT REGIONS IN HIGH CURRENT DISCHARGES

2.1 Statement of the Problem

Because of the complicated nature of the problem, it is desirable to first outline the technique of solution and clarify the phenomenological approach. The full solution should result in the following information:

1) The power absorbed by the electrode.
2) The electrode configuration that will give best performance for any specific requirement.
3) The attachment area of the discharge to the electrode. If two or more possible solutions exist (e.g. point attachment or diffuse attachment) the solution should indicate the conditions under which each will occur.
4) The formation of multiple spot attachment should be predicted and the reason for its occurrence explained.
5) The material loss rate from the electrode should be predicted.

The above information should be obtained with the following quantities as parameters:

1) The arc current.
2) The ambient gas pressure.
3) The properties of the electrode material, e.g., electrical resistivity, melting point, thermal conductivity, etc.
4) The properties of the ambient gas, e.g. electrical conductivity, thermal conductivity, etc.

In the literature, the approach to this problem involves the study of three regions. These are:

1) The electrode.
2) The Mackeown layer, contained between the electrode surface and a surface one electron mean free path out from the electrode.

3) The gas or plasma between the outer edge of the Mackeown layer and the arc column.

In this report, we will assume that the gas extends right up to the electrode surface and that no Mackeown layer is necessary to adequately describe the phenomena. This assumption is equivalent to saying that no special significance need be assigned to the energy gained by the charged particles as they pass through the electric field immediately adjacent to the electrode surface. Considerations of this energy in the past have led to the concepts of field ionization vs. thermal ionization in the gas near the electrode surface. The former was postulated to occur when the electrons gain energy through this layer equal to the ionization or excitation energy of the gas. Rather than invoke this process, we will assume that a temperature can always be assigned to the electrons, even at the surface of the metal. This temperature will depend upon the electric field in the gas, the gas pressure and other quantities. Continuity of electron temperature at the gas-electrode interface is next assumed. One consequence of this assumption is that, near the surface, the electron temperature in the metal must be higher than the temperature of the atom lattice. This concept should be investigated from the point of view of Fermi-Dirac statistics and little can now be said about the depth of penetration of this effect or of the feasibility of it occurring. Another consequence of this is that the electron emission capability of the electrode depends upon the electron temperature, not the atom or lattice temperature in the electrode structure. Field emission of electrons from the electrode is now not a separate mechanism, but is incorporated into the broadened concept of thermionic emission. Some justification for this approach will be discussed in Section 2.2.1 of this report.

The study has now resolved itself into a well defined mathematical problem. The magnetohydrodynamic (MHD) equations must be solved in the electrode and in the gas and the two solutions matched at the interface. This is still a formidable task and many simplifications must be introduced into the analysis before we can expect to obtain closed

form solutions. A general procedure will be outlined in the following sections of this report, but only the simplest problem will be solved. Even this solution is expected to give us some information concerning electrode behavior.

2.2 Mathematical Formulation of the Problem

2.2.1 Current Density at the Electrode Surface

One of the most difficult problems that confronts any theorist who tackles the problem of electrode phenomena in high intensity arcs is that of explaining the high current density observed to occur at the cathode of many arcs. The Richardson equation for current density is usually several orders of magnitude lower than the observed values if the temperature used in the equation is the melting temperature of the cathode or lower. The usual direction out of this dilemma is to invoke field emission and/or the Auger effect as mechanisms to enhance the current carrying ability of the surface. The former requires fields of the order of 10^8 volts/m and the latter requires ion flux rates into the cathode comparable to the electron flux rate out of the surface. Often both of these assumptions appear unrealistic. It is also difficult to start with a realistic set of equations and show that such conditions can actually occur. In order to arrive at a set of usable equations, we will adopt a different approach. First, it is assumed that the electrode surface temperature can rise above the melting point of the material, and in some cases, even above the boiling point. When the electrode is the cathode, it is not necessary to conclude that this will necessarily result in a large loss rate of material, as the vapor which enters the discharge can be quickly ionized and carried back to the electrode surface as ions by the electric field force. (See Fig. 1). On the other hand, there is no such mechanism to prevent the loss of material from the anode and, for this reason, we expect it to be more difficult to keep anodes from eroding. Second, we shall assume that the electron temperature can be higher than the gas or material temperature and that the Richardson equation can be written as:

$$j = 2|e| \left(\frac{kT_e}{2\pi m_e} \right)^{1/2} \left(\frac{2\pi m_e kT_e}{h^2} \right)^{3/2} \exp \left\{ - \frac{|e|\chi}{kT_e} \right\} \qquad (1)$$

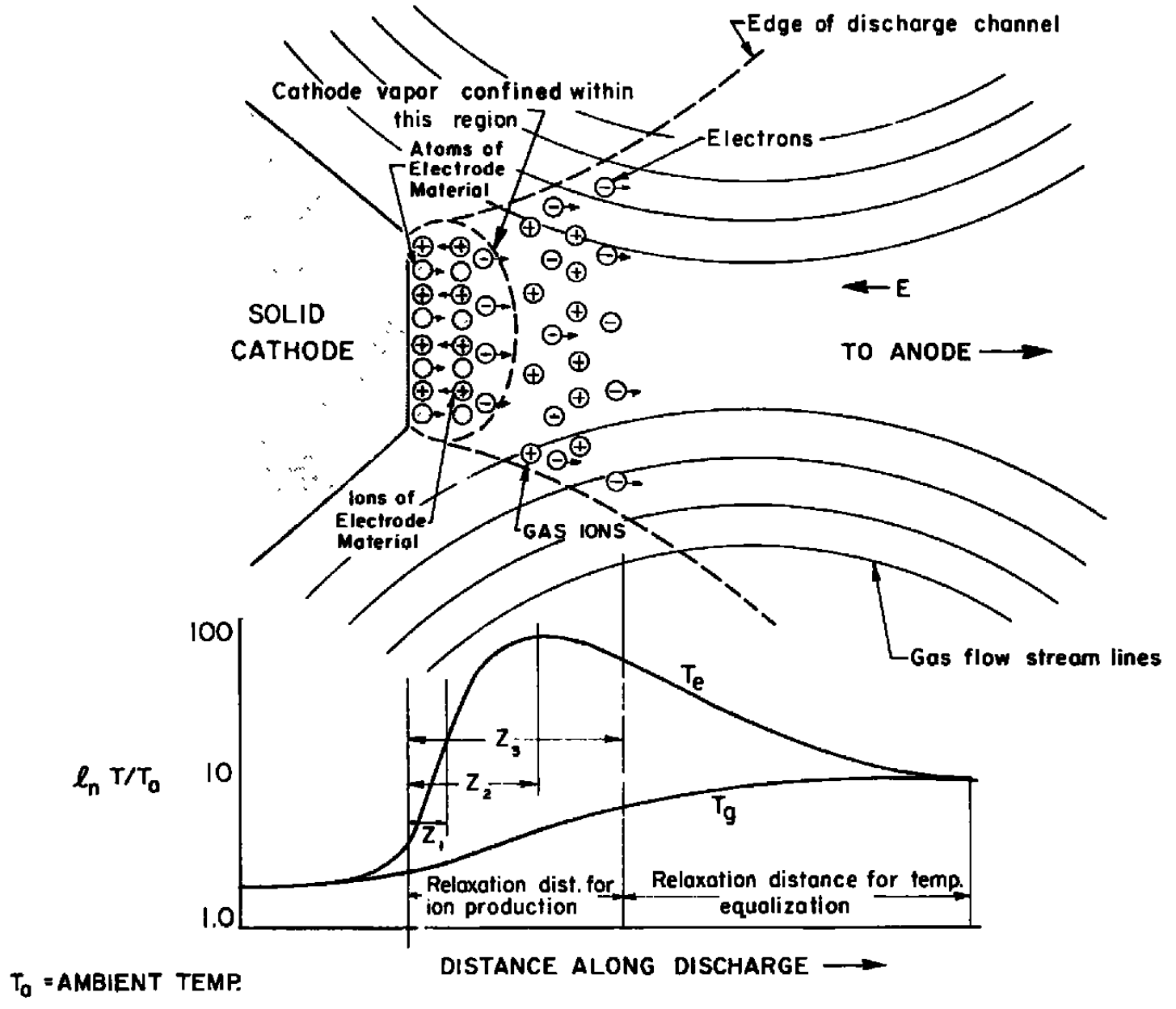

FIG. 1 POSTULATED CATHODE MECHANISMS

Some calculations are carried out below to indicate that this assumption is not unreasonable.

The current density for the electrons at the surface is determined by assuming that a reasonably strong field can carry off all the electrons that would strike the surface due to thermal motion if no field were present. The significant temperature in evaluating this quantity is clearly the electron temperature:

$$j = \frac{|e|\, n_e}{4} \left(\frac{8kT_e}{\pi m_e} \right)^{1/2} \tag{2}$$

The electron density is now determined by equating the electron chemical potential inside the surface to the electron chemical potential outside the surface.

$$(\mu_e)_{inside} = |e|\chi \tag{3}$$

$$(\mu_e)_{outside} = kT_e \ln \frac{2}{n_e} \left\{ \left(\frac{2\pi m_e kT_e}{h^2} \right)^{3/2} \right\} \tag{4}$$

Once again, it appears reasonable to use the electron temperature, T_e, in the definition of the electron chemical potential outside of the metal. Combining these three expressions, the modified form of the Richardson equation as shown in Eq. (1) is obtained.

Further indications as to the reasonableness of this approach,can be obtained by applying the formula to the emission of electrons into a vacuum in the presence of strong applied electric fields. In this case we define the electron temperature as the mean electron energy in that plane parallel to the electrode surface where the force on the electrons is equal to zero. When the only forces acting on the electrons are the image forces and the electric field force, then the electron temperature can be found to be:

$$kT_e = kT_s \left\{ 1 + \frac{1}{kT_s} \left(\frac{|e|^3 E}{4\pi \epsilon_o} \right)^{1/2} \right\} \tag{5}$$

When $\frac{1}{kT_s}\left(\frac{|e|^3 E}{4\pi \varepsilon_o}\right)^{1/2} < 1$, the current density equation can be written as:

$$j = (j)_o \exp\left\{\left(\frac{|e|^3 E}{4\pi\varepsilon_o}\right)^{1/2} \frac{1}{kT_s}\right\} \tag{6}$$

which is the equation describing the Schottky effect.

When the distance between the electrode surface and the plane where the force on the electrons is equal to zero becomes of the order of the electron wave length, then quantum mechanics must be used to describe the emission characteristics of the electrode. The distance between the surface and the critical plane can now be written as:

$$\lambda = \frac{h}{m_e u} \tag{7}$$

The electron energy at the surface must be

$$|e|\ \chi = \frac{1}{2} m_e u^2 \tag{8}$$

If we now put

$$kT_e = kT_s + |e|\ E\lambda \tag{9}$$

then

$$kT_e = kT_s + \frac{|e|\ E\ h}{(2|e|\ m_e\ \chi)^{1/2}} \tag{10}$$

When the second term on the right hand side is large compared to the term kT_s, then the current density equation can be written as:

$$j = \frac{\pi\ |e|^2\ E^2}{h\chi} \exp\left\{-\frac{(2\ |e|\ m_e)^{1/2}\ \chi^{3/2}}{E\ h}\right\} \tag{11}$$

This equation should be compared with the Fowler-Nordheim equation for field emission shown below:

$$j = \frac{|e|^2 E^2}{2\pi h \chi} \exp\left\{ - \frac{8\pi}{3} \frac{(2|e| m_e)^{1/2} \chi^{3/2}}{Eh} \right\} \qquad (12)$$

The relations are remarkably similar. The exponent in the expression derived here from simple considerations is lower than the Fowler-Nordheim value by $\frac{8\pi}{3}$. It is probably completely fortuitous that experiments indicate the Fowler-Nordheim exponent should be reduced by about this value.

2.2.2 Equations to Solve in the Electrode

Fortunately, only one equation, that of the energy balance, needs to be solved in the electrode material

$$\nabla \cdot (\kappa \nabla T) + \rho_M j^2 = 0 \qquad (13)$$

Boundary conditions are needed to determine the solution. In this report, we shall give the temperature at the interface and the temperature of the electrode at some position distant from the interface. The latter will either be at infinity, or at some position where the electrode is cooled. Lateral surfaces are assumed to be thermally insulated. The solution to this problem then gives parametric relations among the following quantities:

1) The arc current.
2) The surface area of attachment.
3) The heat flux rate across the surface from the gas into the electrode.
4) The surface temperature of the electrode.
5) The geometric terms which describe the electrode configuration.

One rather general solution to this problem will be given in Section 3.1.

2.2.3 Equations to Solve in the Gas

The strong electric fields that can occur in the electrode attachment regions indicate that non-equilibrium phenomena can be important in describing the phenomena. A set of complete non-equilibrium equations of a partially ionized gas have been derived in Ref. 2 . These equations, modified to include more than one species of gas, will be used to study the gaseous region of the attachment zone.

A number of fairly general assumptions can be made initially so that considerable simplification is introduced into the problem. These are outlined below:

1) Some vapor of the electrode material is always present in the electrode attachment region of high intensity electric discharges unless the resonance or minimum excitation potential of the ambient gas is lower than that of the electrode vapor. When no vapor is present, it is assumed that the

discharge is operating in a "glow discharge" mode rather than the arc mode. The importance of this assumption lies in the fact that the minimum excitation potential of most metal vapors is of the order of 2-4 volts. This permits ionization of the metal vapor to occur in multiple stages by collision with electrons of relatively low energy, hence, in some cases, the electron temperature does not have to be much above the surface temperature of the electrode, e.g., a tungsten surface at 3600 ^{o}K. The surface temperature of the electrode is now allowed to rise significantly above the melting point of the material and, in high pressure discharges, can even rise above the boiling point of the material (greater than 6000 ^{o}K for tungsten).

2) The attachment region is assumed to lie close enough to the surface so that no forced convection can occur in this zone. The velocity vector in the gas region is then only that resulting from the net loss rate of material from the surface.

3) No external magnetic fields will be considered initially. Only the self-magnetic field of the discharge will be used. This then allows the use of axially symmetric coordinates to describe the attachment region.

4) It has been observed that cathodes can operate for hundreds of hours with a negligible loss of material, although the surface has been melting. From this observation, we make the basic assumption that the material vaporized from the surface is ionized rapidly and returned to the surface by the electric field force, thus resulting in a zero net loss rate of cathode material. The mechanisms are shown schematically in Fig. 1. This assumption greatly simplifies the analysis and eliminates the need to study the heavy particle species diffusion equations.

3. ENERGY BALANCE

The energy balance at the cathode can be divided into two separate problems that are related through the matching of boundary conditions at the interface between the gas and metal electrode. The first, and easier of the two problems is a study of the balance between thermal conduction and energy dissipation in the metal electrode. The second problem is to study the balance among thermal conduction, energy dissipation, energy radiation and energy convection in the gas. This is an extremely complicated problem and general solutions are not easy to find. The mathematical formulation of these two problems will be discussed in the following sections and some solutions for specific configurations will be worked out.

3.1 Energy Balance in the Metal

The basic assumption made in studying this problem is that the discharge attaches to the cathode on a small area. The problem of balancing the dissipation and heat flow can then be formulated in spherical coordinates and a model postulated as shown in Fig. 2. Here the discharge attaches at r_o and heat flows radially inward from this position. When the angle θ is equal to 90^o, this model can then be used to describe the case when a discharge attaches to a point on a plane electrode. The differential equation in spherical coordinates is as follows:

$$\frac{1}{r^2}\frac{d}{dr}\left(r^2 \mathcal{K} \frac{dT}{dr}\right) + \rho\, j^2 = 0 \qquad (14)$$

In this expression, $\rho = \frac{1}{\sigma}$ = the resistivity of electrode material and is assumed to be a function of the local temperature only. In order to linearize the equation, a new variable, the thermal conduction integral, is introduced as follows:

$$\phi = \int_o^T \mathcal{K}\, dT \qquad (15)$$

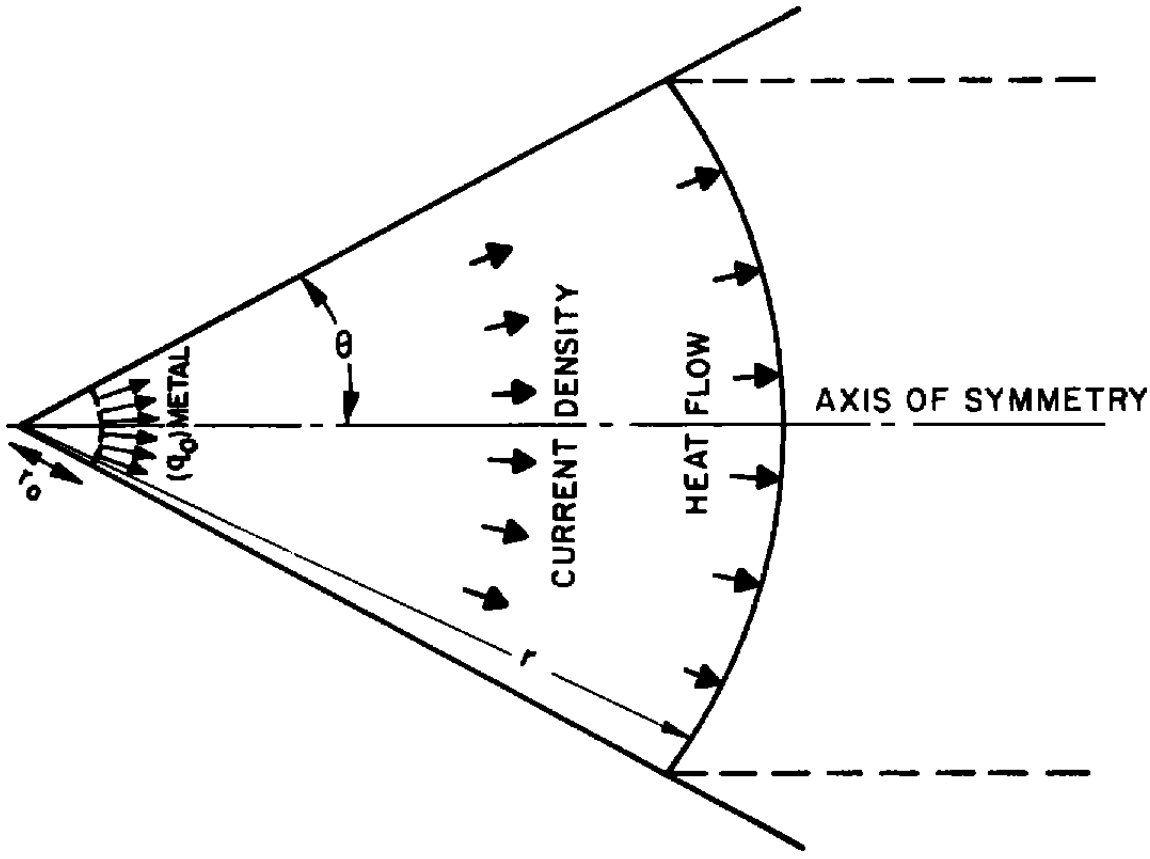

FIG. 2 MODEL USED FOR SOLVING THE ENERGY EQUATION IN THE ELECTRODE

Since the electrical resistivity is assumed constant over each surface at a constant value of r, it is possible to replace the current density by the total current:

$$j = \frac{I}{2\pi r^2 (1 - \cos \theta)} \tag{16}$$

The next assumption which is made is that a linear relation can be found between the thermal conductivity integral ϕ and the electrical resistivity ρ. For most substances, such an assumption is realistic over a reasonable range of temperature. The relation between the thermal conductivity integral and the metal temperature is shown in Figs. 3 and 4 for tungsten and copper, respectively. Figs. 5 and 6 show how good the linear approximation between ϕ and ρ is for tungsten and copper. The straight line approximation cuts the ϕ axis at some value ϕ'. Because of this, it is better to define a new variable as follows:

$$\bar{\varphi} = \int_{T'}^{T} K dT = \phi - \phi' \tag{17}$$

where T' is the temperature at which $\phi = \phi'$. With this definition, $\rho = \left(\frac{d\rho}{d\phi}\right) \bar{\varphi}$.

The differential equation can now be written:

$$\frac{1}{r^2} \frac{d}{dr} \left(r^2 \frac{d\bar{\varphi}}{dr}\right) + \frac{I^2 \frac{d\rho}{d\phi} \bar{\varphi}}{\left[2\pi r^2 (1 - \cos \theta)\right]^2} = 0 \tag{18}$$

This equation can be easily integrated as follows:

Put

$$\frac{I \left(\frac{d\rho}{d\phi}\right)^{1/2}}{2\pi (1 - \cos \theta)} = r' \tag{19}$$

Then

$$\frac{d^2}{d\left(\frac{r'}{r}\right)^2} \bar{\varphi} + \bar{\varphi} = 0 \tag{20}$$

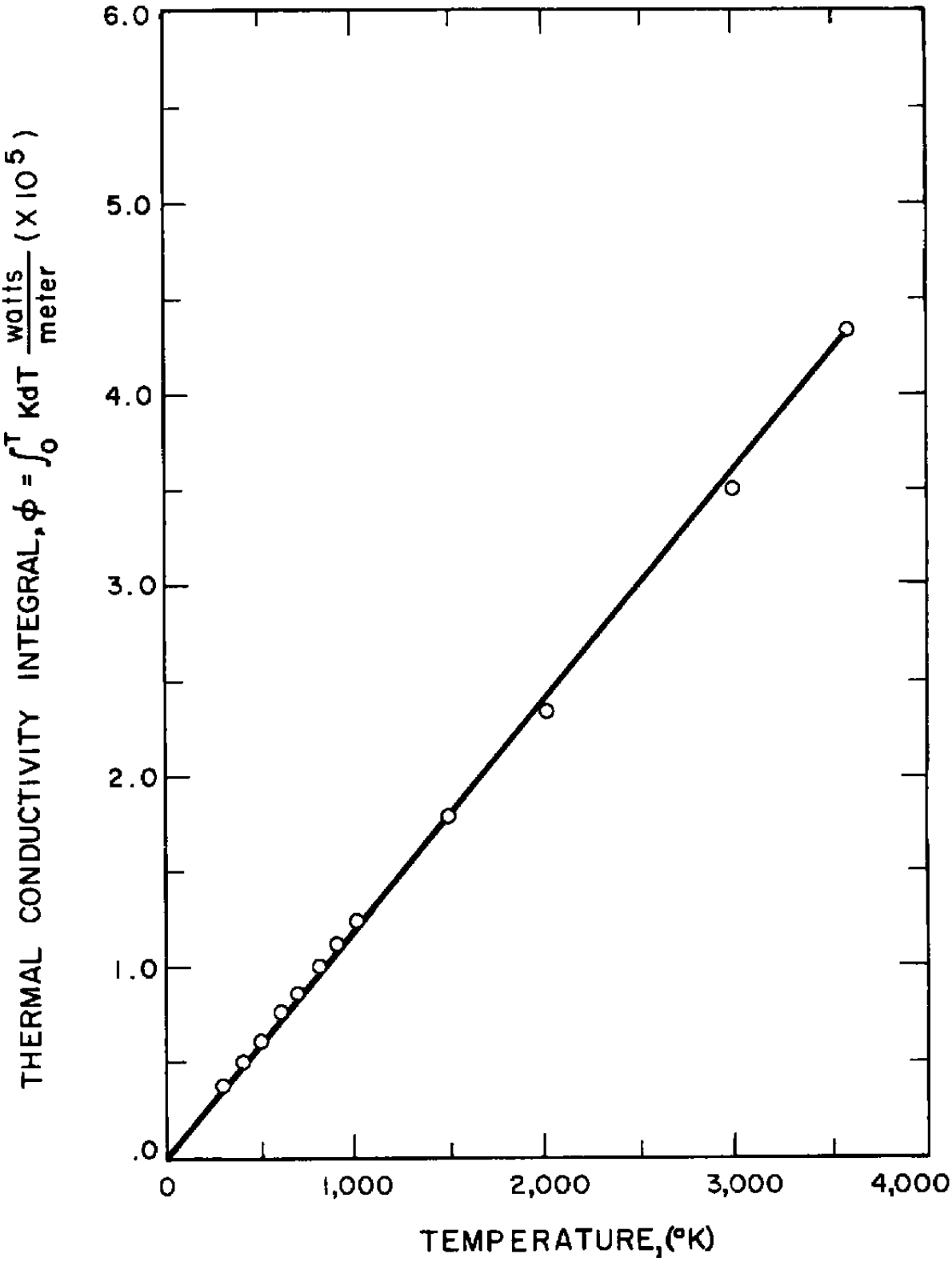

FIG. 3 THERMAL CONDUCTIVITY INTEGRAL VS TEMPERATURE FOR TUNGSTEN (Determined from Data of Ref. 4)

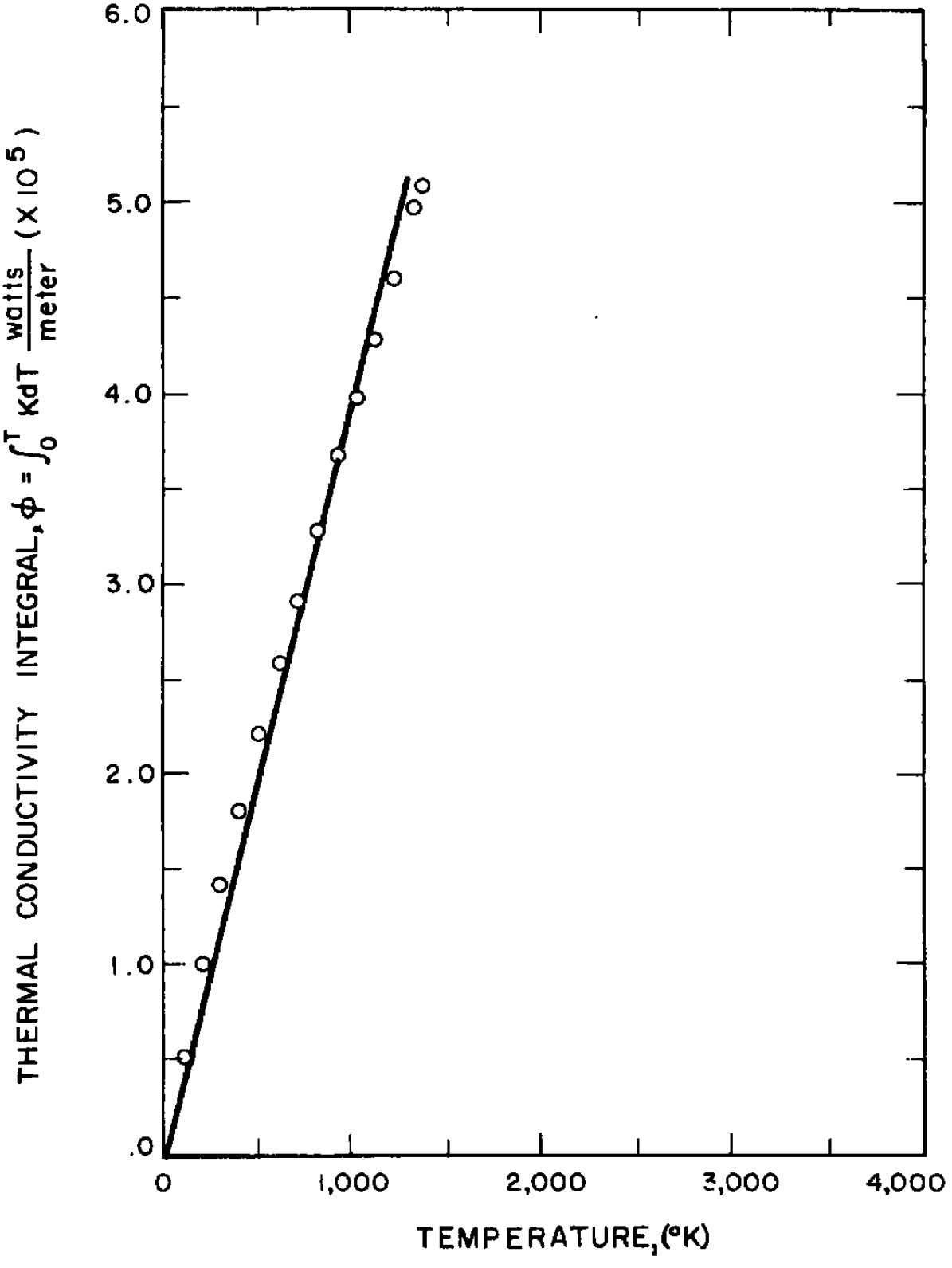

FIG. 4 THERMAL CONDUCTIVITY INTEGRAL VS TEMPERATURE FOR COPPER (Determined from Data of Ref. 4)

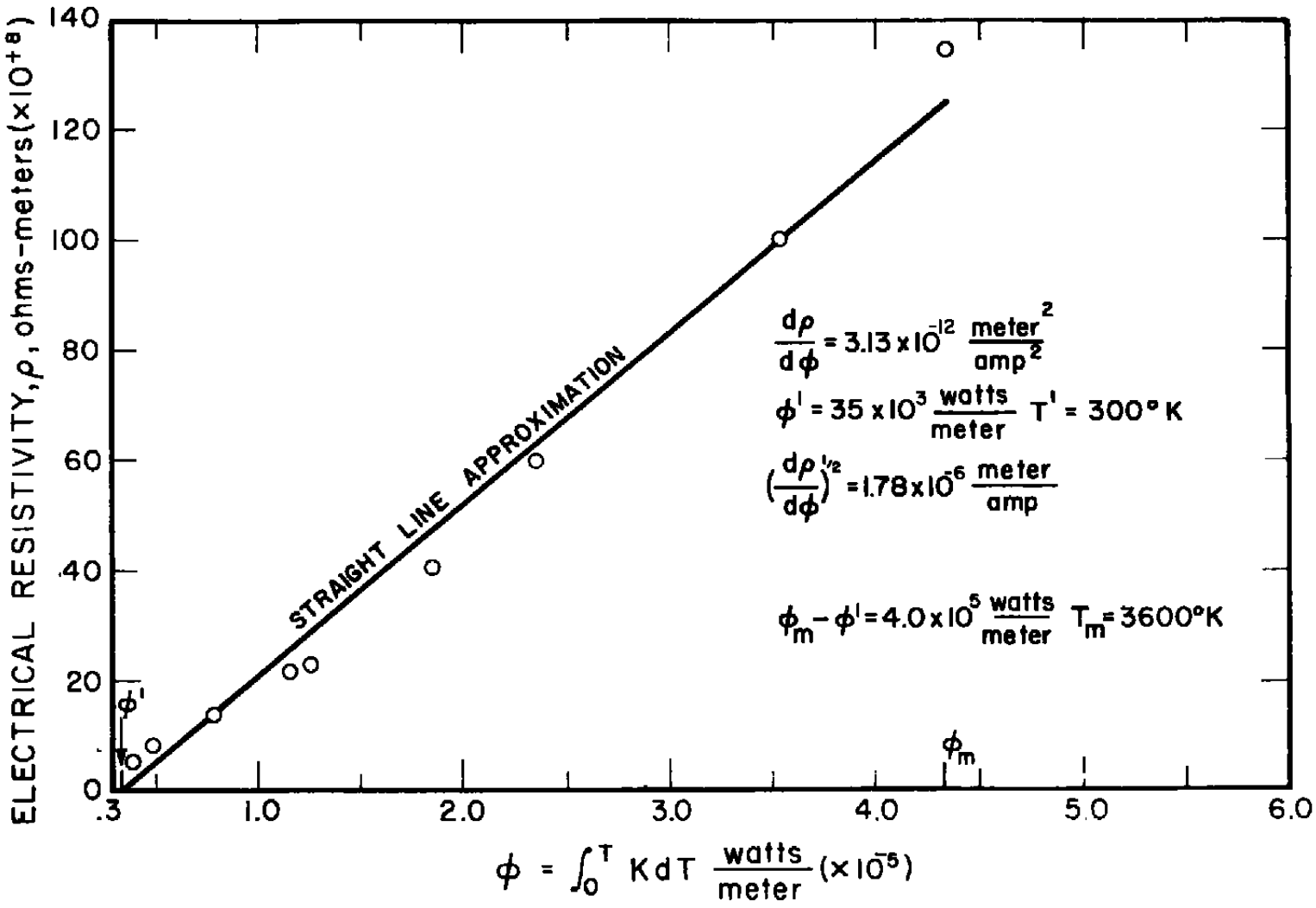

FIG. 5 ELECTRICAL RESISTIVITY OF TUNGSTEN VS Φ (Determined from Data of Ref. 4)

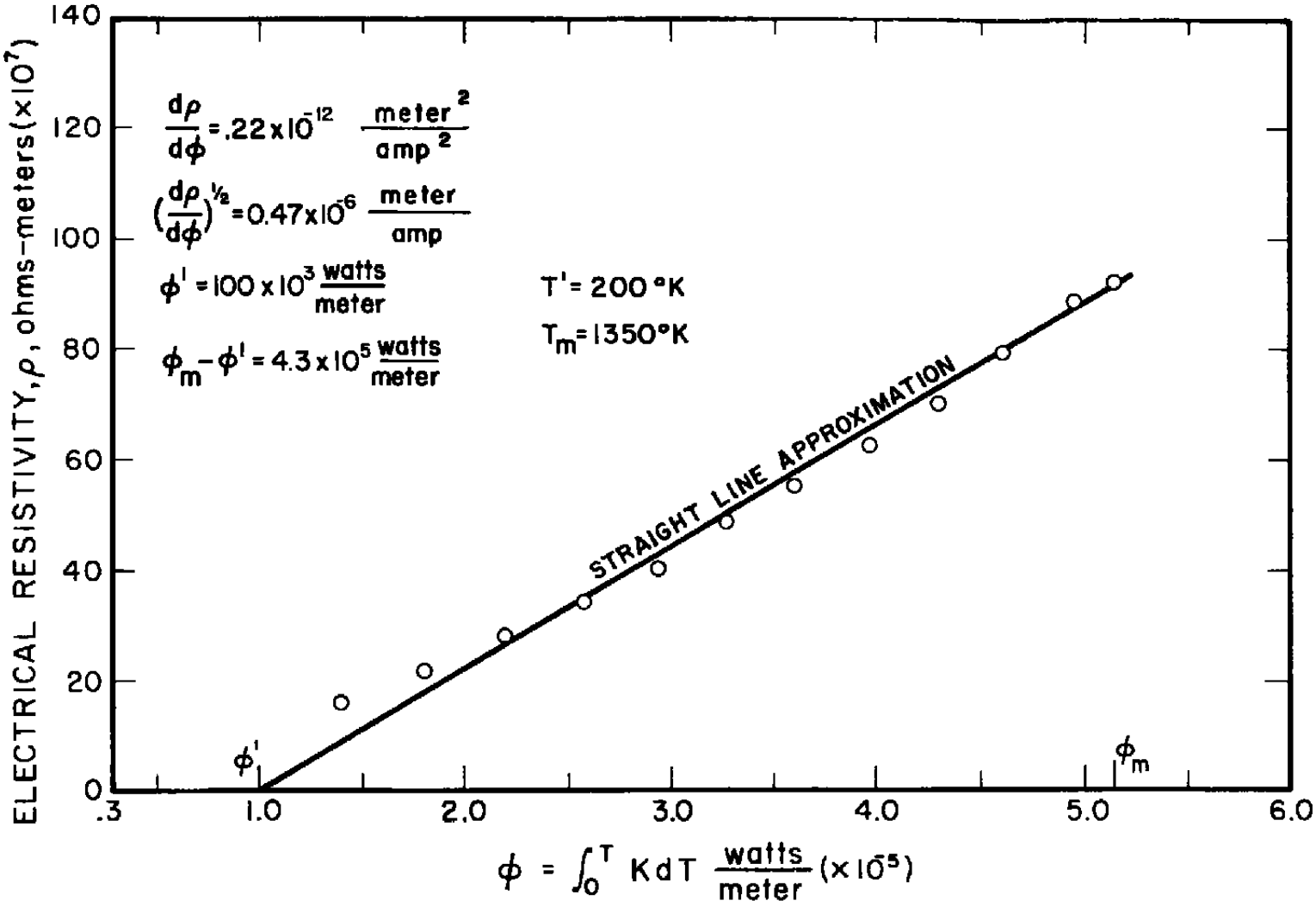

FIG. 6 ELECTRICAL RESISTIVITY OF COPPER VS Φ (Determined from Data of Ref. 4)

The general solution of which is:

$$\Phi = \Phi_1 \cos \frac{r'}{r} + \Phi_2 \sin \frac{r'}{r} \tag{21}$$

The values of Φ_1 and Φ_2 are determined by the boundary conditions, which will usually be evaluated at the attachment point in terms of the surface temperature and heat flux rate into the metal. The heat flux rate can be found by differentiating the expression for Φ

$$q = -\frac{d\Phi}{dr} = -\frac{r'}{r^2}\left[\Phi_1 \sin \frac{r'}{r} - \Phi_2 \cos \frac{r'}{r}\right] \tag{22}$$

This expression can be written more conveniently in terms of the power transferred across each cross-section

$$P = I\left(\frac{d\rho}{d\Phi}\right)^{1/2}\left(\Phi_2 \cos \frac{r'}{r} - \Phi_1 \sin \frac{r'}{r}\right) \tag{23}$$

In practice, the cathode will be cooled by some technique, e.g., water at some radius, r_w. This would then allow us to apply one boundary condition at r_o and one at r_w. In order to obtain some simple, yet important parametric relations, it will be assumed that the cooling is done as $r_w \to \infty$ and thus $\Phi_1 = 0$. The following relations now hold at the attachment point.

$$(\Phi_o)_{metal} = \Phi_2 \sin \frac{r'}{r_o} \tag{24}$$

$$q_o = r' \frac{\Phi_2}{r_o^2} \cos \frac{r'}{r_o} \tag{25}$$

$$P_o = I\left(\frac{d\rho}{d\Phi}\right)^{1/2} \Phi_2 \cos \frac{r'}{r_o} \tag{26}$$

Combining the first two equations, the following relation is obtained:

$$\frac{2\pi\ (1 - \cos\ \theta)\ \bar{\varphi}_o}{q_o\ I\ \left(\frac{d\rho}{d\bar{\varphi}}\right)^{1/2}} = \frac{r_o^2}{(r')^2}\ \tan\frac{r'}{r_o} \tag{27}$$

The radius of the arc attachment spot is $r_o \sin\theta$. Using this relation the heat flux into the metal can be written as:

$$(q_o)_{metal} = \frac{\sin^2\theta\ \left(\frac{d\rho}{d\phi}\right)^{1/2}\ I\ (\phi_o)_{metal}}{2\pi(1 - \cos\theta)\ r_{arc}^2\ \tan\left[\frac{(\sin\theta)\left(\frac{d\rho}{d\phi}\right)^{1/2} I}{2\pi(1-\cos\theta)\ r_{arc}}\right]} \tag{28}$$

The power which enters the electrode at the surface and through internal dissipation is conducted away. The total power (which would go into any cooling system) is given by

$$P_{electrode} = \frac{I\ \left(\frac{d\rho}{d\phi}\right)^{1/2}\ (\bar{\varphi}_o)_{metal}}{\sin\left[\frac{(\sin\theta)\ \left(\frac{d\rho}{d\phi}\right)^{1/2}\ I}{2\pi\ (1-\cos\theta)\ r_{arc}}\right]} \tag{29}$$

The expressions derived above are expected to be approximately valid even for the case of an arc attachment to a plane electrode in which case $\theta = \frac{\pi}{2}$.

3.2 Heat Balance in an Arc Near the Attachment Point

We assume that a cylindrical arc (see Fig. 7) is attached to an electrode, and that in the immediate vicinity of the attachment there is no convection. Power dissipated by ohmic heating is carried away by radiation and conduction. The equation for thermal equilibrium is given by:

$$-\frac{\partial^2 \phi}{\partial z^2} - \frac{1}{r}\frac{\partial}{\partial r}\left(r\frac{\partial \phi}{\partial r}\right) + P_r = j^2/\sigma. \tag{30}$$

Eq. (30) was originally derived for arcs with axial conduction and no convection, and ϕ was the integral of the conductivity with respect to the temperature. The phenomena near the attachment must be such that the electrons are not in equilibrium with the atoms (since the atoms must be approximately at the temperature of the melting electrode which is too low to permit electrical conduction). Hence we say that ϕ is to be some function (related to electron and atom temperatures) such that the heat flux is proportional to the gradient of ϕ. It is further assumed that both P_r and σ (which are due to phenomena similar to heat conduction) vary linearly with ϕ, and go to zero at the same value of ϕ (ϕ is defined to be zero at that condition). Assume that the electric field $j/\sigma = \int j\, dA / \int \sigma dA$. With the above assumptions the equilibrium equation (30) becomes:

$$-\frac{\partial^2 \phi}{\partial z^2} - \frac{1}{r}\frac{\partial}{\partial r}\left(r\frac{\partial \phi}{\partial r}\right) + \frac{dP_r}{d\phi}\phi = \frac{I^2 \phi}{\left(\frac{d\sigma}{d\phi}\right)\left[\int_0^{r_{arc}} \phi\, 2\pi r\, dr\right]^2} \tag{31}$$

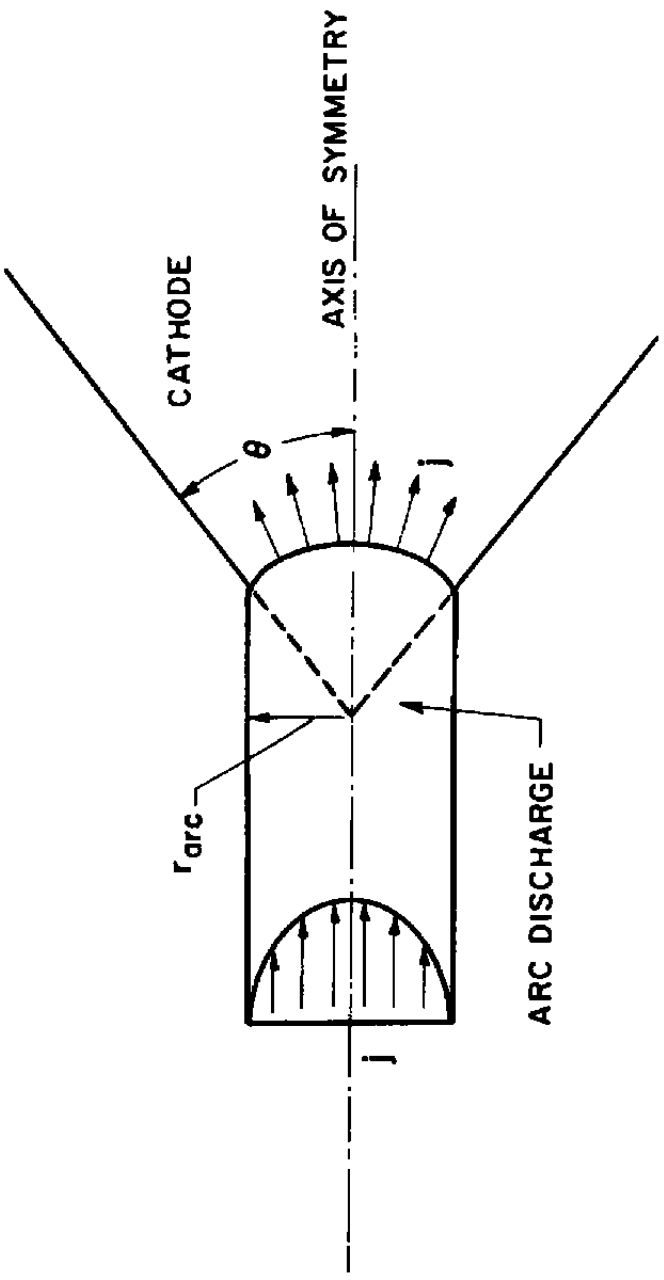

FIG. 7 MODEL USED FOR SOLVING THE ENERGY EQUATION IN THE GAS

A solution has been found for Eq. (31) which satisfies the boundary conditions:

$$\left.\begin{aligned} \phi &= 0 && \text{for } r = r_{arc} \\ \phi &< \infty && \text{for } r = 0 \\ \phi &= \phi_{gas} \frac{2.4\, J_o\left(2.4 \frac{r}{r_{arc}}\right)}{2\, J_1(2.4)} && \text{for } z = 0 \\ \phi &< \infty && \text{for } z \to \infty \end{aligned}\right\} \quad (32)$$

The first of these conditions is that the arc is "cold" at the outside edge, the third gives the average value of ϕ at the attachment, and the fourth condition is sufficient to insure a unique solution for the axial distribution. Under the above conditions, the solution is separable.

Let

$$\phi(r,z) = \frac{I}{(2.4)\,\pi \left(\frac{d\sigma}{d\phi}\right)^{1/2} r_{arc} \left[1 + \left(\frac{r_{arc}}{2.4}\right)^2 \frac{dP_r}{d\phi}\right]^{1/2}} \frac{2.4\, J_o\left(2.4 \frac{r}{r_{arc}}\right)}{2\, J_1(2.4)} \Phi(s) \quad (33)$$

and

$$z = \frac{r_{arc}}{2.4 \left[1 + \left(\frac{r_{arc}}{2.4}\right)^2 \frac{dP_r}{d\phi}\right]^{1/2}} s \quad (34)$$

Using the above substitutions, Eq. (31) reduces to:

$$\frac{d^2\Phi}{ds^2} = \Phi - \frac{1}{\Phi} , \quad (35)$$

where

$$\Phi = \Phi_o \equiv \frac{(2.4)\pi \left(\frac{d\sigma}{d\phi}\right)^{1/2} r_{arc} \left[1 + \left(\frac{r_{arc}}{2.4}\right) \frac{dP_r}{d\phi}\right]^{1/2} \phi_{gas}}{I} \quad \text{at } s = 0, \quad (36)$$

and

$$\Phi < \infty \quad \text{as } s \to \infty.$$

The solution of Eq. (35) is the function $\Phi(s)$ which satisfies

$$\int_{\Phi_o}^{\Phi(s)} \frac{dU}{\sqrt{U^2 + \ln\left(\frac{1}{U^2}\right) - 1}} = s. \quad \text{(See Fig. 8).} \quad (37)$$

The average value of $\frac{2.4\, J_o\left(2.4\, \frac{r}{r_{arc}}\right)}{2\, J_1\,(2.4)}$ over the cross-section is one, hence the average value of ϕ is

$$\phi_{avg} = \frac{I\, \Phi(s)}{(2.4)\pi \left(\frac{d\sigma}{d\phi}\right)^{1/2} r_{arc} \left[1 + \left(\frac{r_{arc}}{2.4}\right)^2 \frac{dP_r}{d\phi}\right]^{1/2}} \quad (38)$$

The average axial conduction heat flux is given by

$$q_{gas} = \left(\frac{\partial \phi}{\partial z}\right)_{avg} = \frac{d}{dz}\left(\phi_{avg}\right) = \frac{I}{\pi\, r_{arc}^2 \left(\frac{d\sigma}{d\phi}\right)^{1/2}} \frac{d\bar{\sigma}}{ds} \quad (39)$$

where

$$\frac{d\Phi}{ds} = \sqrt{\Phi^2 + \ln\left(\frac{1}{\Phi^2}\right) - 1} \quad (40)$$

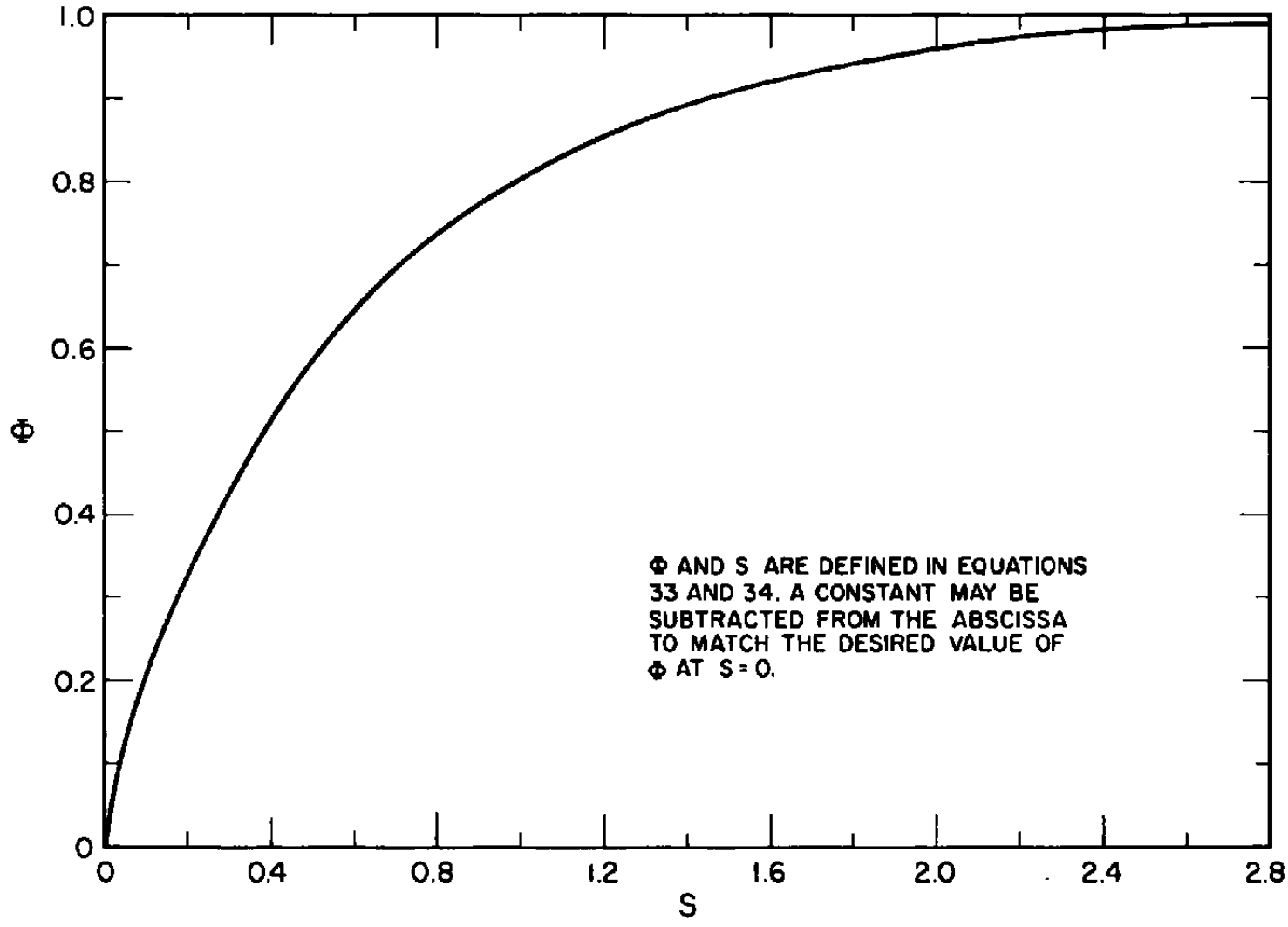

FIG. 8 DIMENSIONLESS CONDUCTIVITY INTEGRAL IN ARC VS DISTANCE FROM CATHODE SURFACE

The field E which is $I/\int c\,dA$ becomes

$$E = \frac{2.4\left[1+\left(\frac{r_{arc}}{2.4}\right)^2 \frac{dP_r}{d\phi}\right]^{1/2}}{r_{arc}\left(\frac{d\sigma}{d\phi}\right)^{1/2}_{\phi}} = \frac{I}{\pi r_{arc}^2 \frac{d\sigma}{d\phi}\phi_{avg}} \qquad (41)$$

3.3 Heat Balance at the Cathode Surface

Solutions have been obtained for relationships between surface temperatures (or ϕ), surface heat flux (q), arc radius and current for both the electrode and the arc (gas). For the metal:

$$(q_o)_{metal} = \frac{\sin^2\theta\left(\frac{d\rho}{d\phi}\right)^{1/2} I\,(\Phi_o)_{metal}}{2\pi\,(1-\cos\theta)\,r_{arc}^2 \tan\left[\frac{\sin\theta\left(\frac{d\rho}{d\phi}\right)^{1/2} I}{2\pi\,(1-\cos\theta)\,r_{arc}}\right]} \qquad (42)$$

For the gas neglecting radiation, the average heat flux is given by:

$$q_{gas} = \frac{I}{\pi r_{arc}^2\left(\frac{d\sigma}{d\phi}\right)^{1/2}}\sqrt{\left(\frac{2.4\pi r_{arc}\left(\frac{d\sigma}{d\phi}\right)^{1/2}\phi_{gas}}{I}\right)^2 + \ln\left(\frac{I}{2.4\pi r_{arc}\left(\frac{d\sigma}{d\phi}\right)^{1/2}\phi_{gas}}\right)^2 - 1} \qquad (43)$$

These heat fluxes differ for two reasons (see Fig. 6). First, there is an area difference. The $(q_o)_{metal}$ applies over a spherical area which is $2/(1+\cos\theta)$ times the cross-section area of the arc. Hence it was divided to match the power (heat flux x area) rather than the flux. Second, there is a heat sink given in terms of the work function χ. The heat balance will be written (neglecting radiation from surface.)

$$(\pi r_{arc}^2)\, q_{gas} = \frac{2}{1+\cos\theta}(\pi r_{arc}^2)\,(q_o)_{metal} + I\,\chi. \qquad (44)$$

It is necessary to obtain information about ϕ_{gas}. ϕ in the arc is related to the field E by:

$$\phi = \frac{I}{\pi r_{arc}^2 \frac{d\sigma}{d\phi} E} \tag{45}$$

Applying this relationship at the surface, ϕ_{gas} can be eliminated in terms of E_s. The resulting heat balance was multiplied by $(\frac{d\sigma}{d\phi})^{1/2}/I$ and the result is:

$$\sqrt{\left(\frac{2.4}{(\frac{d\sigma}{d\phi})^{1/2} E_s r_{arc}}\right)^2 + \ln\left(\frac{(\frac{d\sigma}{d\phi})^{1/2} E_s r_{arc}}{2.4}\right)^2 - 1} \tag{46}$$

$$= \frac{\left(\frac{d\sigma}{d\phi}\frac{d\rho}{d\phi}\right)^{1/2} (\Phi_o)_{metal}}{\tan\left[\frac{\sin\vartheta (\frac{d\rho}{d\phi})^{1/2} I}{2\pi (1-\cos\vartheta) r_{arc}}\right]} + \left(\frac{d\sigma}{d\phi}\right)^{1/2} \chi$$

In order to apply Eq. (46), $(\Phi_o)_{metal}$ was taken to be the melting value(it would not be necessary to do this if more information were available) and the field in the gas near the surface was obtained as follows: The electron current j_e is written in terms of σE

$$j_e = \frac{|e|^2 n_e}{k T} \frac{3}{16}\sqrt{\frac{2\pi kT}{m_e}} \frac{E}{\sum_i n_i q_i} \tag{47}$$

The electron current can also be written in terms of the charge and mean velocity:

$$j_e = n_e |e| \frac{1}{4}\sqrt{\frac{8 kT}{\pi m_e}} \tag{48}$$

Eliminating j_e we get:

$$E = \frac{8\ kT}{3\pi\ |e|} \sum_i n_i\ q_{ei} \tag{49}$$

The sum of products of number density and cross-section is over values for gas atoms and ions of electrode material. The number densities are related to the partial pressures, and the total pressure is equal to the pressure at the outside plus the average magnetic pinch pressure.

$$kT\Sigma n_i q_i = (n_a k\ T)\ q_{ea} + (n_I\ kT)\ q_{eI} \tag{50}$$

$$= P_a\ q_{ea} + P_I\ q_{eI}$$

$$P_a + P_e + P_I = P_a + 2P_I = P_o + \frac{\mu_o\ I^2}{8\pi^2\ r_{arc}^2} \tag{51}$$

Combining the above, we get:

$$E_s = \frac{8}{3\pi\ |e|}\left[\left(P_o + \frac{\mu_o\ I^2}{8\pi^2\ r_{arc}^2}\right) q_{ea} + P_I\ q_{eI}\right], \tag{52}$$

where q_{ea} has been neglected compared to q_{eI}. q_{ea} and q_{eI} are given in terms of the temperature. P_I can be found since it is the vapor pressure of the electrode material. Eq. (52) can be used to eliminate E_s from Eq. (46). This equation now has two unknowns, I and r_{arc} (P_o and Temp are considered known). I and r_{arc} are related by

$$j = \frac{1 + \cos\ \theta}{2}\ \frac{I}{\pi\ r_{arc}^2}, \tag{53}$$

where j is a function of T (from the Richardson equation or a plot of thermionic emission). See Figs. 9 and 10.

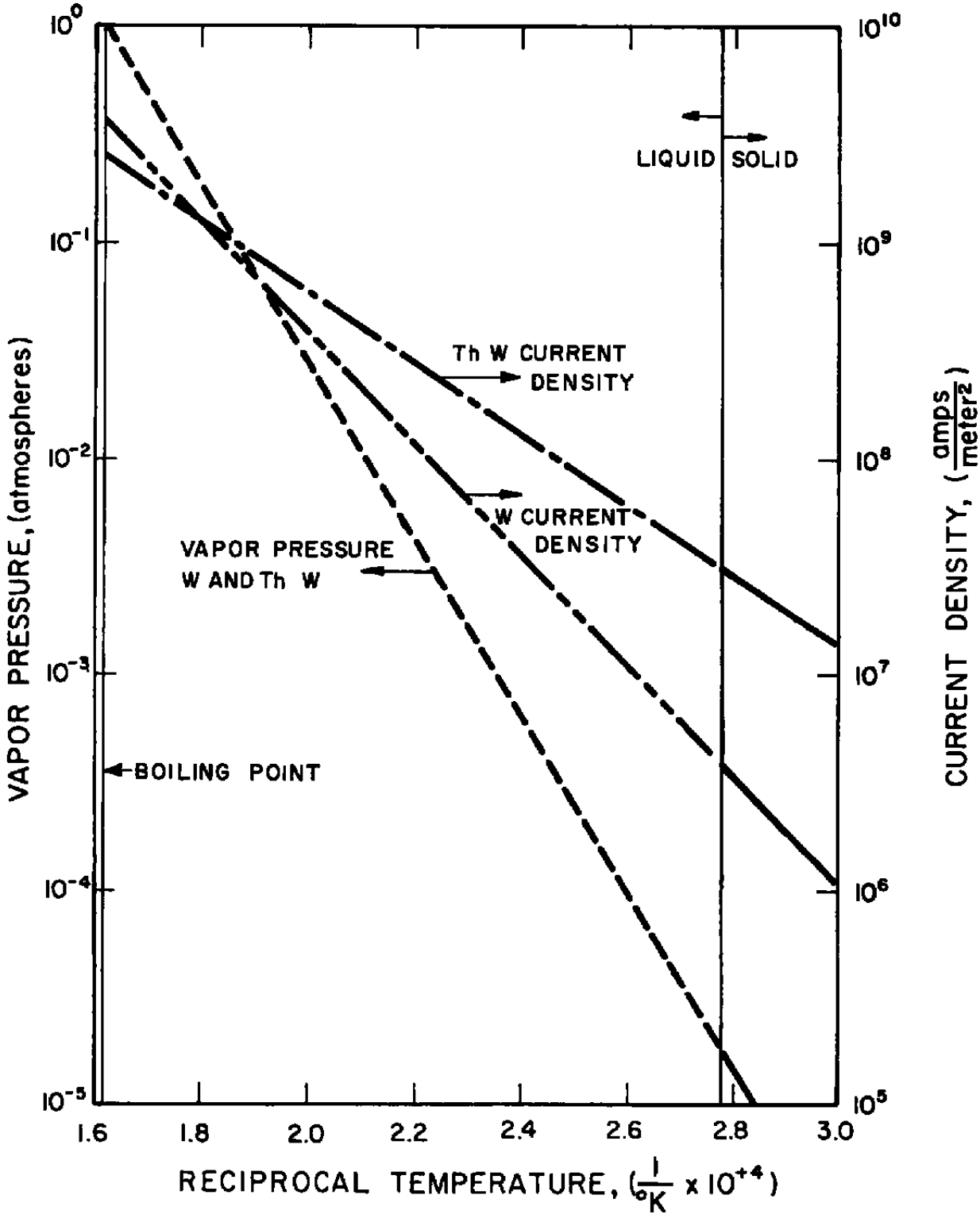

FIG. 9 VAPOR PRESSURE AND THERMIONIC EMISSION CURRENT DENSITY FOR TUNGSTEN (Determined from Data of Ref. 5)

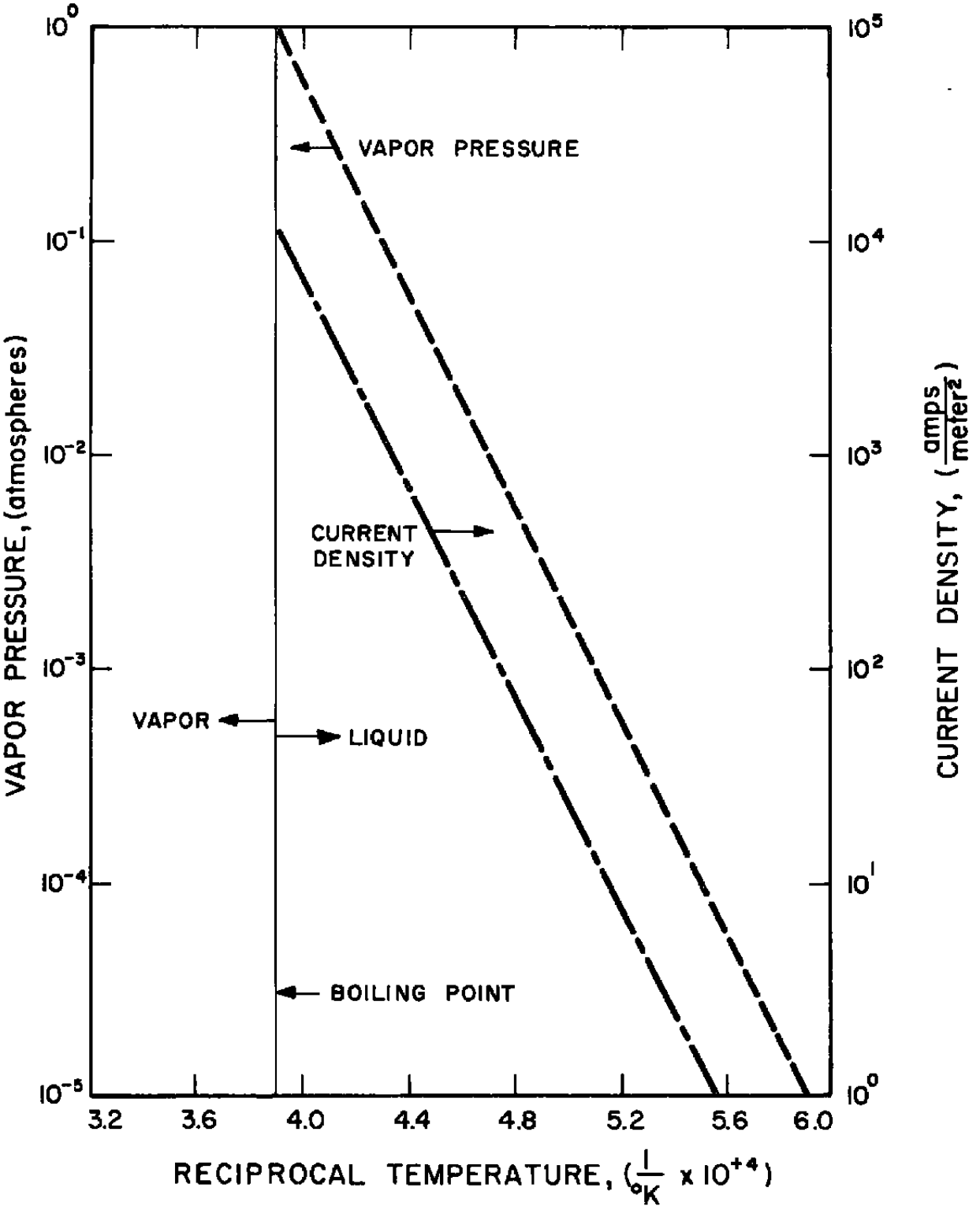

FIG. 10 VAPOR PRESSURE AND THERMIONIC EMISSION CURRENT DENSITY FOR COPPER (Determined from Data of Ref. 5)

The problem then has a solution, which is a value for I, r_{arc}, E_s and $P_{cathode}$, etc., for each value of P_o and surface temperature. Figs. 11 and 12 show typical solutions.

3.4 Heat Balance at the Anode Surface

The problem for the anode is very similar to that of a cathode. The principal difference is that the work function is a negative number. Also, it is the anode material atoms (not ions) which are present in the arc, and hence in Formula 52, replace q_{eI} by $(q_{ea})_{anode\ material}$.

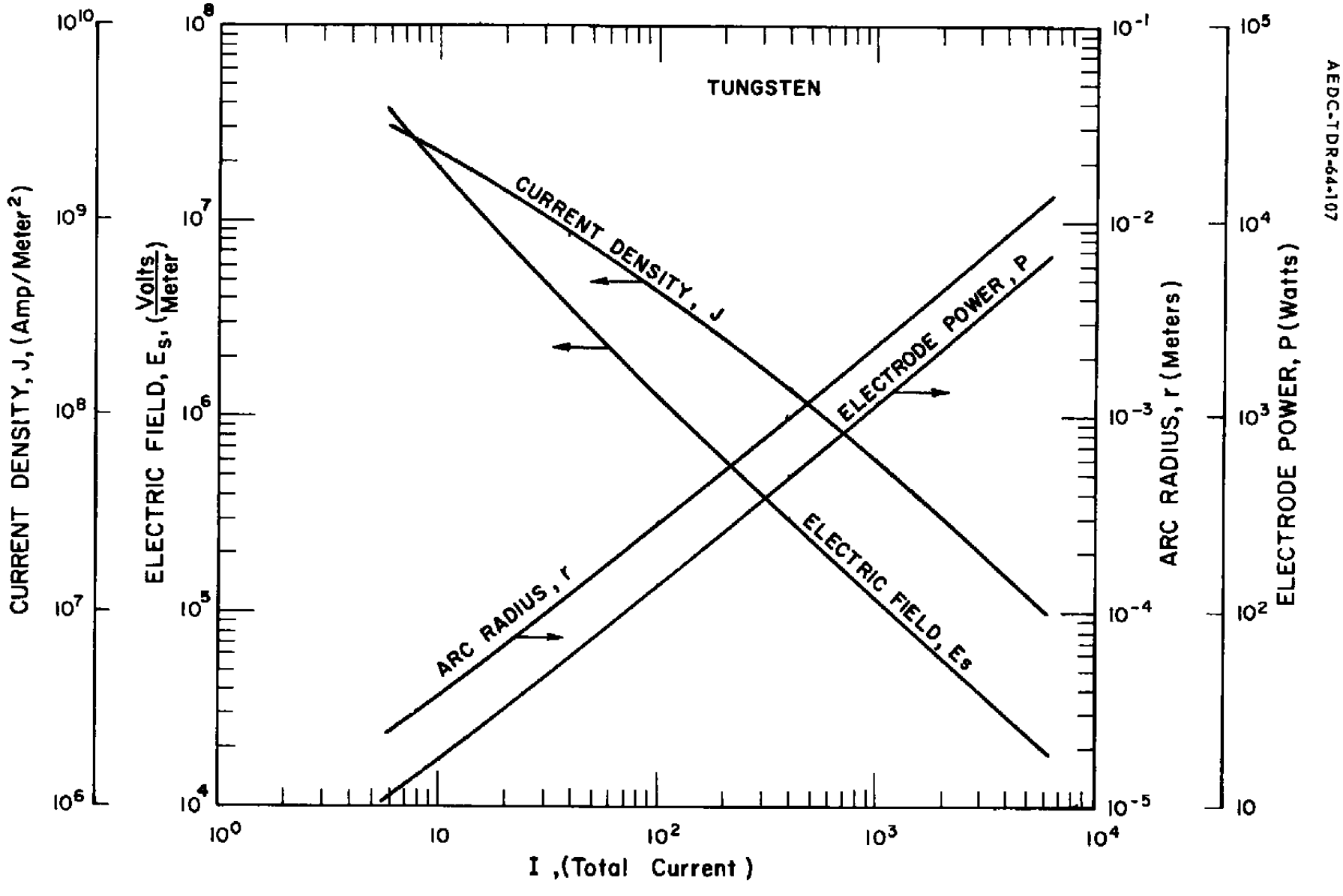

FIG. 11 THEORETICAL SOLUTIONS FOR TUNGSTEN CATHODE

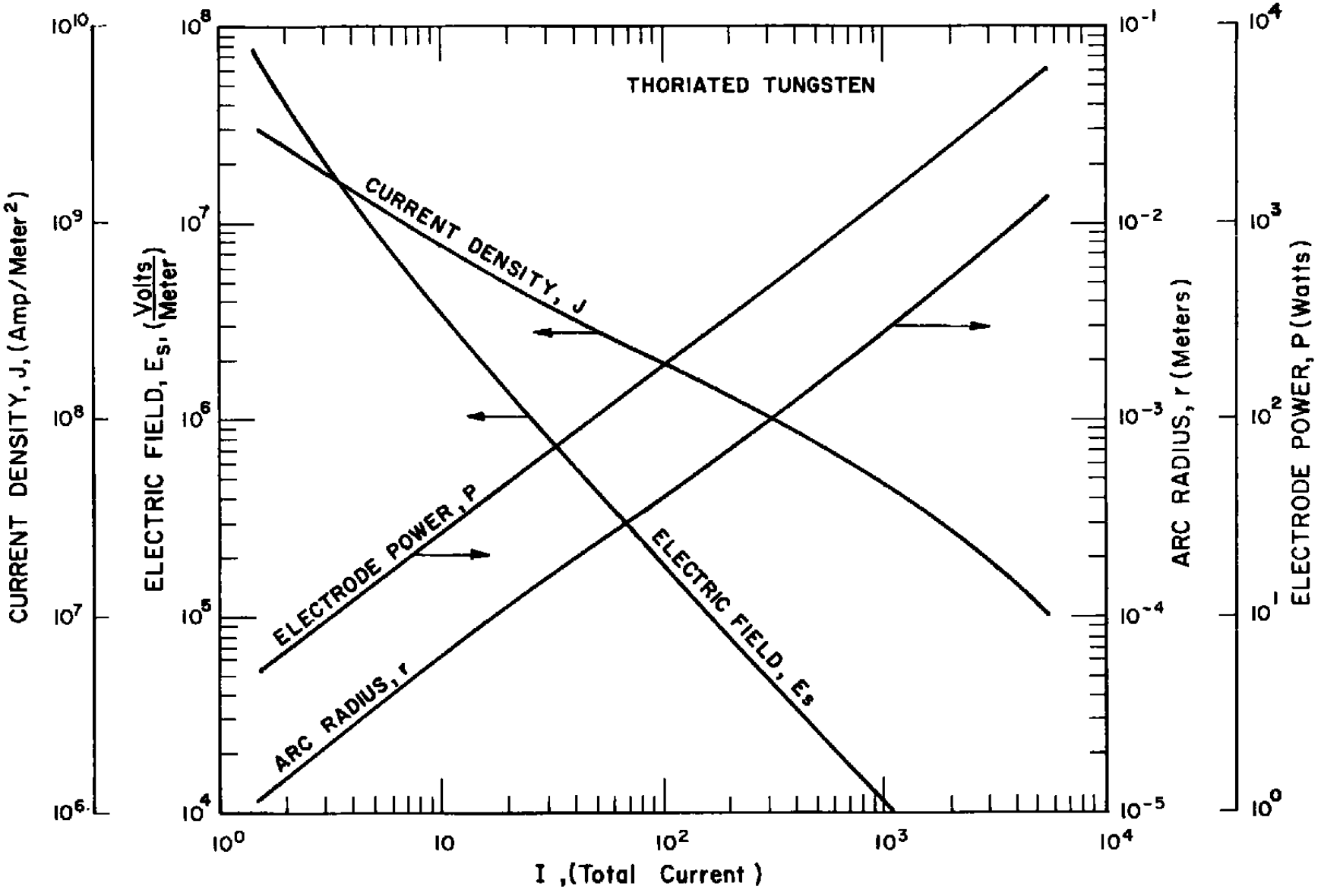

FIG. 12 THEORETICAL SOLUTIONS FOR THORIATED TUNGSTEN CATHODE

4. CATHODE SPOT EXPERIMENT

The theory for the attachment of arcs in high pressure gases to metal electrodes as developed in Section 3 predicts some quantities which can be measured. The power absorbed by the electrode is the one quantity that can be measured with accuracy and compared to the predicted values. Most other measurable quantities, e.g., arc spot size and surface temperature, involve either elaborate equipment to make the measurement or some rather broad assumptions in order to interpret the measurement. Accordingly, an experiment was set up to measure the power lost to an arc cathode under closely controlled conditions. Since the pressure appears as a parameter in the theory, the equipment was designed so that it could be operated at pressure of from 1 mm Hg up to 2 atmosphere.

4.1 Test Geometry

The apparatus for experimental investigations of the cathode attachment region required the solution of many design problems before a satisfactory unit was constructed. These problems arose mainly from the conflicting requirements of good visibility of the attachment region and of confining the arc to form a stable operating configuration. Use of buffers and magnetic fields to stabilize the arc resulted in obscuration of the attachment zone and other operating problems. Deletion of these components for improved visibility resulted in the formation of coatings on the transparent chamber wall and unstable operation under some circumstances. The final configuration chosen was a bare cathode in which the arc was stabilized by the injection of high velocity gas very close to the cathode tip. This configuration is shown schematically in Fig. 13. Photographs of the test geometry assembly and its components are shown in Figs. 14, 15 and 16. While this unit gave satisfactory performance for the most part, coating of the chamber walls persisted and interfered with pyrometer and spectroscope measurements.

The principles of operation of this device are similar to conventional arc heaters. Gas enters a plenum in a phenolic housing

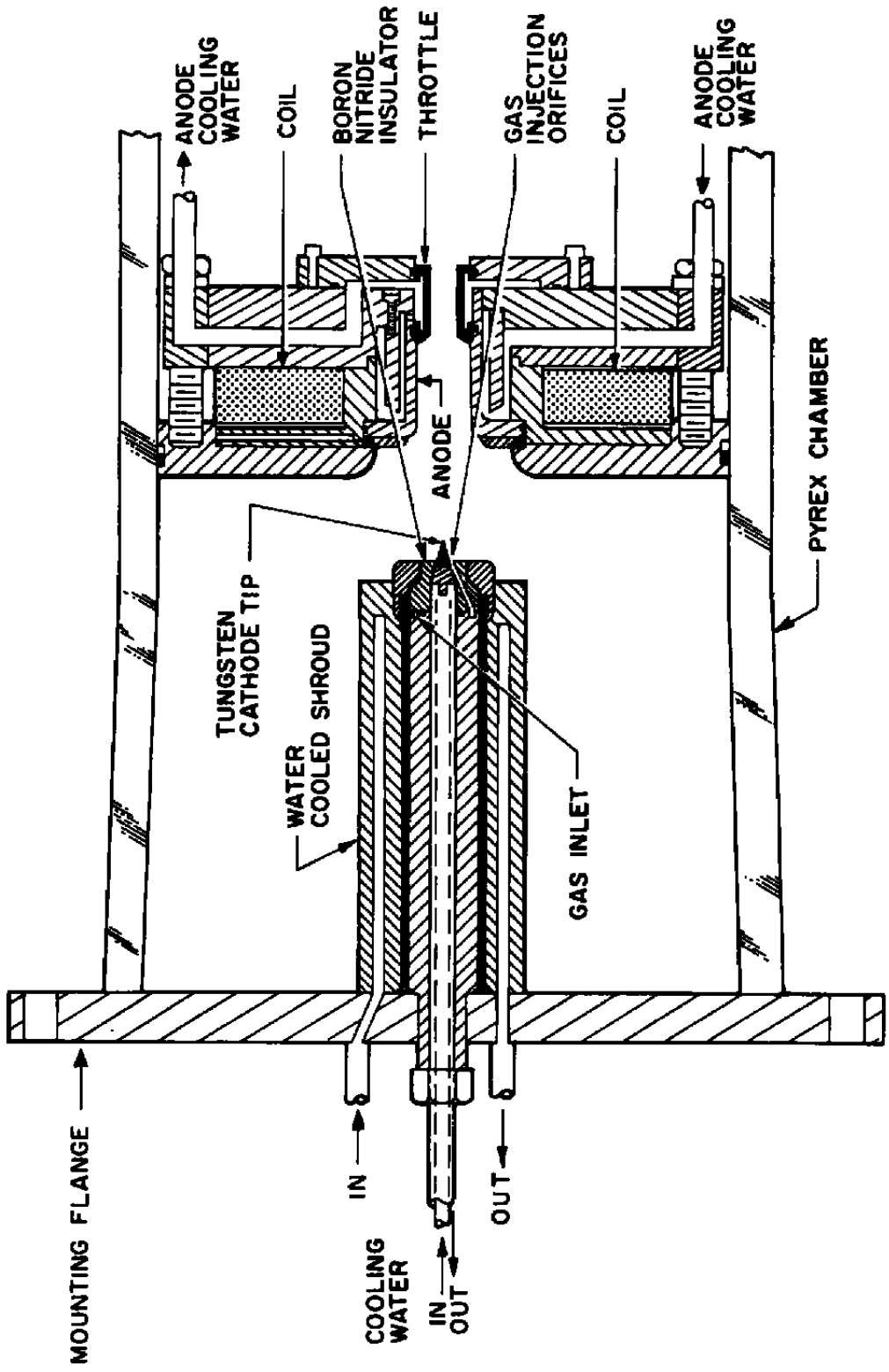

FIG. 13 SCHEMATIC DRAWING OF CATHODE TEST APPARATUS

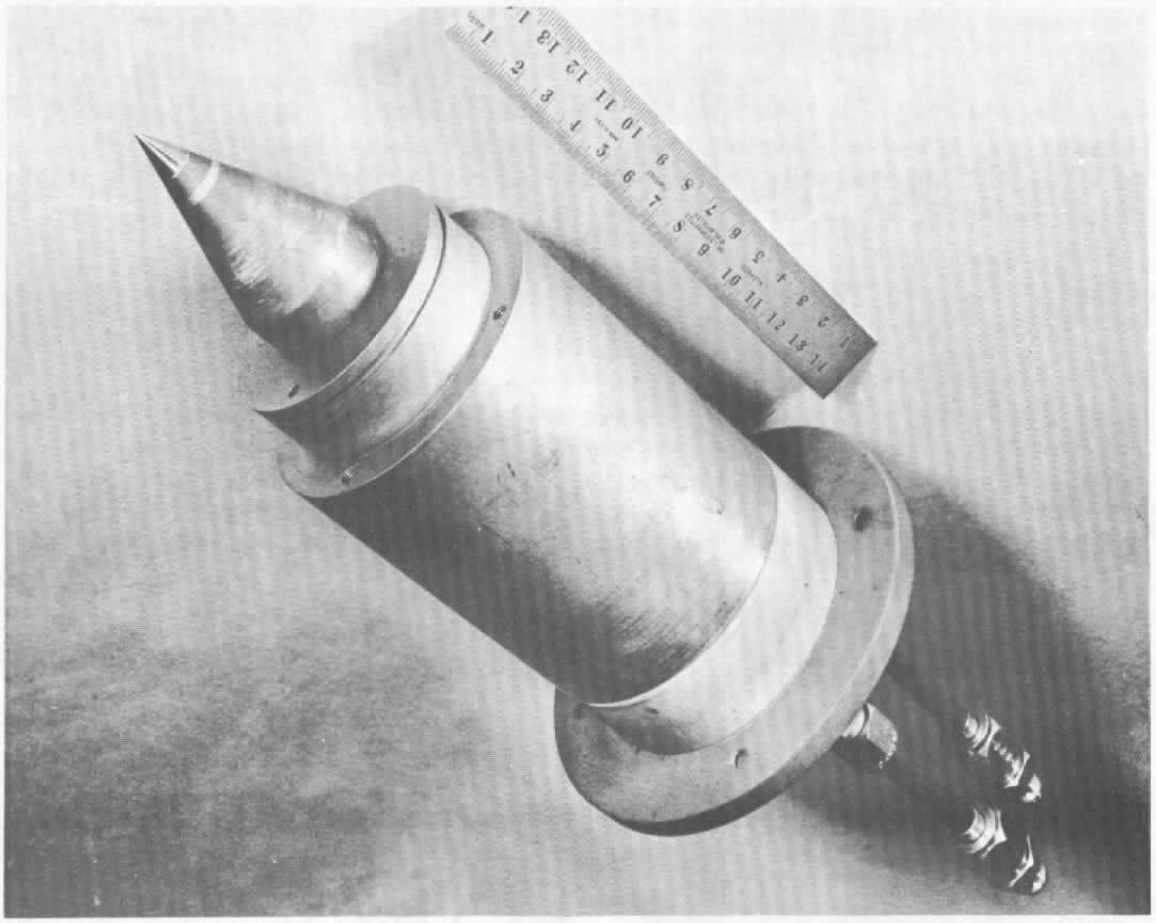

FIG. 14 EARLY ARC CATHODE ASSEMBLY

FIG. 15 COMPONENTS FOR ARC CATHODE STUDY

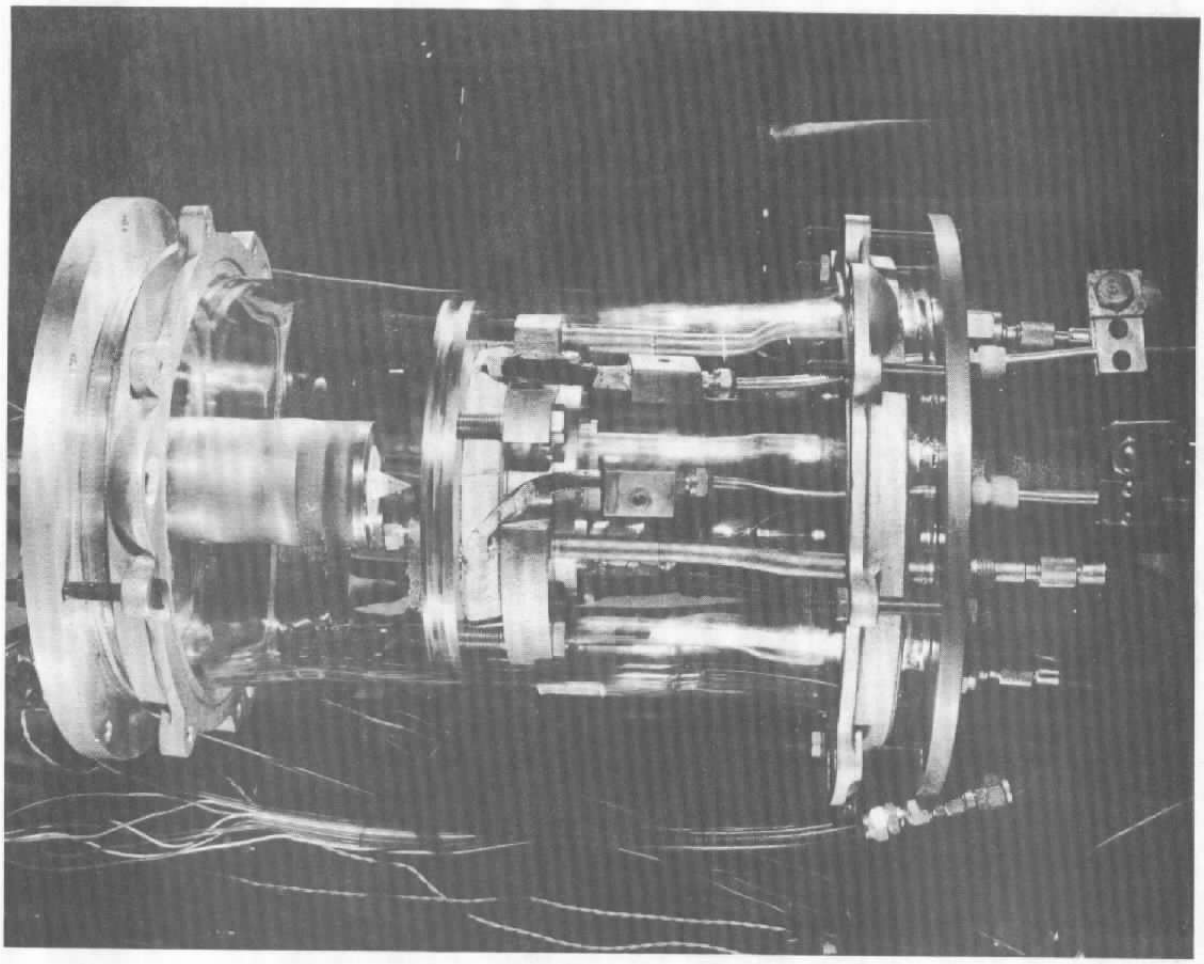

FIG. 16 ASSEMBLED EQUIPMENT FOR CATHODE STUDY

that contains the cathode assembly. Orifices in a boron nitride insulator-positioning block provide passages for the gas from the plenum to the cathode tip. The velocity vector at the point of injection forms a 45° angle with the plane of the axis, providing high velocity, vortex flow over the tip. Cooling water for the cathode tip and cathode housing are provided at the mounting flange. The coolant flows, in addition to maintaining wall temperatures at reasonable values, provide a means for determining the heat loss to the cathode.

The arc is struck from the cathode to an annular anode which is also water cooled. An axial magnetic field produced by the coils interacts with the arc current to provide a rotation of the anode attachment point reducing the local heat flux. Finally a throttle is provided to control the chamber pressure and flow rate. The heated gas is exhausted to a vacuum system. Fig. 17 shows the cathode and column operating in a stable mode with argon as the heated gas.

4.2 Instrumentation

The instrumentation used in these tests is summarized in Table I. These measuring techniques have been evolved and previously used at EOS for accurate determinations of the performance of arc jet propulsion devices. A complete discussion of these and other arc jet measurement techniques is given in Ref. 3.

4.3 Experimental Results

Fig. 18 shows some results of the above experiment for argon. The power in the cathode cooling system is plotted versus the current, and the results are compared with the theory. Also shown on the same figure are additional data for a similar configuration in a hydrogen arc jet. (Unpublished EOS Data).

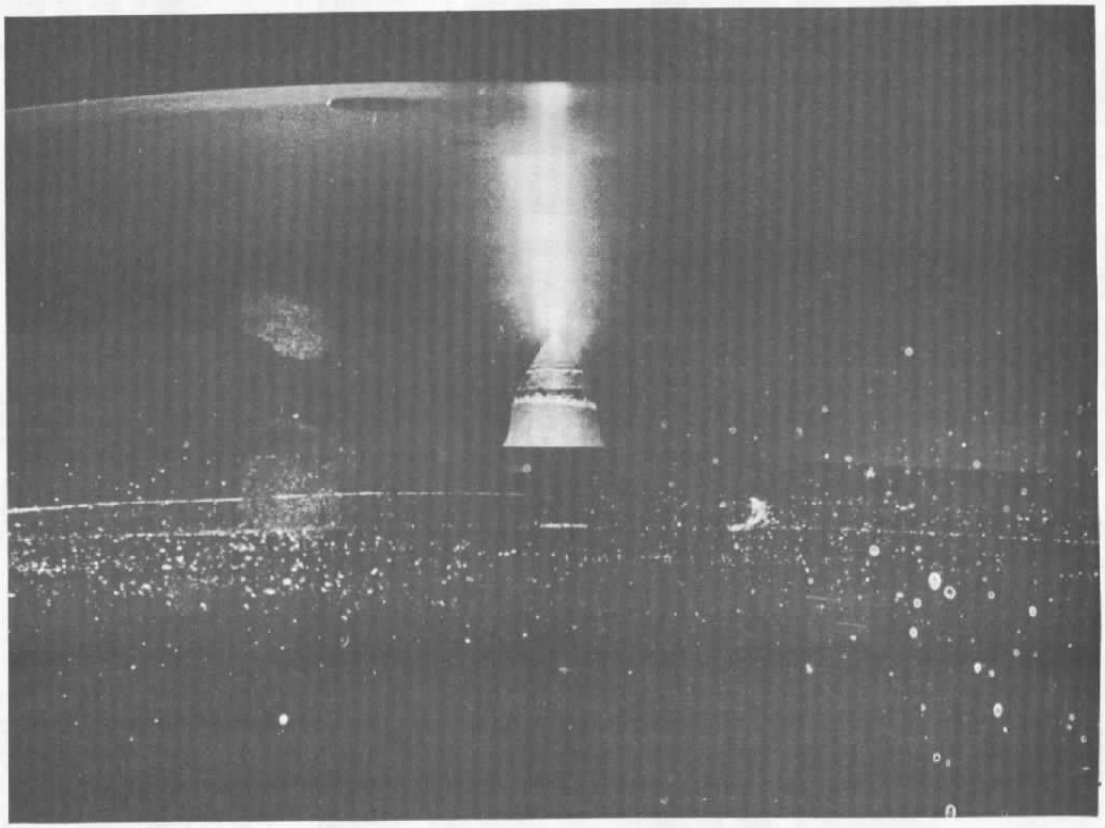

FIG. 17 CATHODE ATTACHMENT AND COLUMN DURING OPERATION

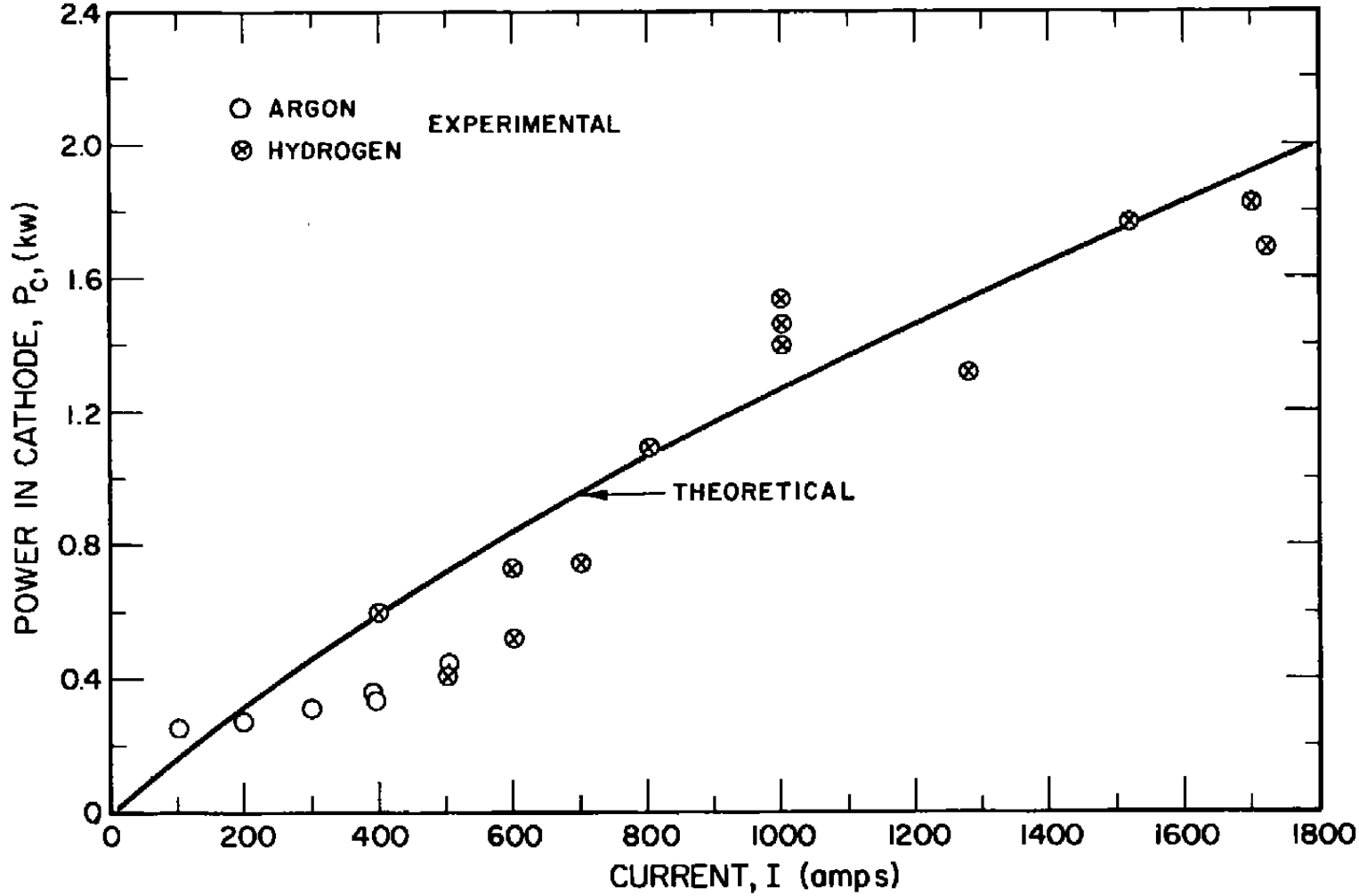

FIG. 18 COMPARISON OF MEASURED AND THEORETICAL VALUES FOR CATHODE POWER

TABLE I

	Measurement	Instrument (Manufacturer)	Range	Accuracy (Calibration Method)
1.	Cathode Voltage	Voltmeter (Rowan) Oscilloscope	0 - 500 v	± 1/2%
2.	Cathode Current	Ammeter (Rowan) Oscilloscope	0 - 1000 a	± 1/2%
3.	Gas Flow	Sonic Orifice and Helix Gage Transducer	Unlimited	1 - 2% (Collection in Meteorological Balloon)
4.	Coolant Flow	ASME Orifice with Hg Manometer, Rotameters	Unlimited	1/2% (Direct Weighing)
5.	Coolant Temperature - Differential	Copper-Constantan t.c.'s in Differential Electrical Circuits. Laboratory Potentiometer (L & N)	na	1/2% (Mfg. Guarantee)
6.	Visual Record of Cathode Spot	High Speed Motion Picture (Fastax - WF3)	8000 fps max.	na
7.	Chamber Pressure	Bourdon Type Gage (Wallace and Tierman)	0-50 mm	1/4%
8.	Discharge Spectra	Spectrograph f 6.3 (Jarrel-Ash)		
9.	Total Radiation	Optical Pyrometer		1%

5. RETROGRADE MOTION OF THE CATHODE SPOT

When the work described in this report was initiated, it was felt that a study of the retrograde motion might help in understanding some of the basic mechanisms occurring in the cathode attachment region. The investigations carried out in the previous sections slowly led us to the conclusion that this was not true and that the retrograde effect basically resulted from effects outside the attachment region. However, a few of the analytic results obtained during the time that we studied the retrograde effect will be presented and the experimental equipment built to measure some critical phenomena predicted by us to be present when motion occurs will be described.

5.1 Analysis of Retrograde Effect

From the outset, we adopted the hypothesis that retrograde motion results from forces on the volume of the ionized gas in the discharge and is not a surface effect. Starting from this, it is possible to use equations for the ambipolar motion of the charged particles through a partially ionized gas and solve in general terms for the velocity of these particles in a discharge when electric and magnetic fields are applied.

The general equation for ambipolar diffusion in a partially ionized gas is given in Ref. 2 and is reproduced below with a few changes of notation.

$$J + \omega_e \tau_e \frac{J \times B}{|B|} - \omega_e \tau_e \omega_I \tau_I \frac{(J \times B) \times B}{|B|^2} = n_I |e| \left\{ \omega_I \tau_I \left(\frac{F_1 - F_2}{|B|} - \frac{F_1}{(1 + \beta_1)\,|B|} \right) + (\omega_e \tau_e \omega_I \tau_I) \left(\frac{(F_1 - F_2) \times B}{|B|^2} \right) \right\} \tag{54}$$

where:

$$\frac{\omega_e \tau_e}{|B|} = \frac{|e|}{kT} D_{ea} \frac{n \dfrac{q_{ea}\, f_{eI}^{(2)}}{q_{eI}\, f_{ea}^{(2)}}}{n_I + n_a \dfrac{q_{ea}\, f_{eI}^{(2)}}{q_{eI}\, f_{ea}^{(2)}}} \tag{55}$$

$$\frac{\omega_I \tau_I}{|B|} = Z_I \frac{|e|}{kT} D_{Ia} \frac{n_a n}{(n_a + n_I)^2} \tag{56}$$

$$F_1 = E + v \times B + \frac{kT}{|e|} (\nabla \ln p_e + K_e \nabla \ln T) \tag{57}$$

$$F_2 = \frac{kT}{|e|} \left\{ \nabla \ln \frac{p_e\, p_I}{p_a} + (K_e - K_I) \nabla \ln T \right\} \tag{58}$$

$$\beta_1 = \frac{n_a}{n_I} \frac{q_{ea}\, f_{eI}^{(2)}}{q_{Ie}\, f_{ea}^{(2)}} \tag{59}$$

J = charge particle flux

Equation (54) can now be changed into a form where the J x B and (J x B) x B terms are replaced by terms including the electric and magnetic fields. After some algebra, the following expression is obtained:

$$M + \left\{ \frac{\left(L_1 + \frac{|B| \mathcal{J}}{\omega_e \tau_e} \right) \cdot B}{1 + \beta_1} \right\} \frac{B}{|B|}$$

$$= \frac{1}{c^2} \left\{ Q - \frac{\omega_e \tau_e}{1 + \omega_e \tau_e \omega_I \tau_I} \frac{Q \times B}{|B|} - (Q \cdot B) \frac{B}{|B|^2} \right. \tag{60}$$

where

$$M = \frac{J|B|}{\omega_I \tau_I} - |e| n_I (F_1' - F_2) - \frac{\beta_1}{1 + \beta_1} \frac{|e| n_I v |B|}{\omega_e \tau_e} \tag{61}$$

$$L_1 = |e| n_I F_I' = |e| n_I (F_1 - v \times B) \tag{62}$$

$$\mathcal{J} = |e| n_I v \tag{63}$$

$$c^2 = \frac{(1 + \omega_e \tau_e \omega_I \tau_I)^2 + (\omega_e \tau_e)^2}{1 + \omega_e \tau_e \omega_I \tau_I} \tag{64}$$

$$Q = \omega_e \tau_e \omega_I \tau_I |e| n_I (F_1' - F_2) + \frac{|e| n_I F_1'}{1 + \beta_1}$$

$$+ \omega_e \tau_e |e| n_I v |B| \left[1 + \frac{\beta_1}{1 + \beta_1} \frac{1 + \omega_e \tau_e \omega_I \tau_I}{(\omega_e \tau_e)^2} \right] \tag{65}$$

In order to obtain a relation connecting the various components of the ion velocity that is valid in an electric discharge with a transverse magnetic field it is convenient to make two simplifying assumptions as follows:

1) The components of v, F_1', and F_2 in the direction of the applied magnetic field can be neglected.
2) $(\beta_1/1 + \beta_1)\ (1/\omega_e \tau_e) \ll 1$, and
3) $(\beta_1/1 + \beta_1) \left[(1 + \omega_e \tau_e \omega_I \tau_I)/(\omega_e \tau_e)^2\right] < < 1.$

The relation shown below can now be obtained from Eq. (65) if a configuration is picked in which the electric discharge is along the y axis and the applied magnetic field is in the z direction.

$$U_x = \frac{(\omega_e \tau_e)^2 \omega_I \tau_I}{1 + (\omega_e \tau_e)^2 + \omega_e \tau_e \omega_I \tau_I} \left[U_y + \ldots \right.$$

$$\left. \ldots + \frac{1 + (\omega_e \tau_e)^2}{(\omega_e \tau_e)^2} \frac{(F_1' - F_2)y}{|B|} + \frac{v_x}{\omega_I \tau_I} + \frac{\omega_e \tau_e F_{1y}' - F_{1x}'}{(\omega_e \tau_e)^2 |B|} \right] \qquad (66)$$

where U = absolute velocity of ions and electrons moving together, i.e., charged particle motion which carries zero electric current. Because of this definition, the x-component of U represents the absolute velocity of the cathode spot.

If the only gas velocity present is v_x, that due to the electromagnetic forces, then U_y is the diffusion velocity of the ions in the + y-direction due to the applied electric field. The arc should then move in the + x-direction since all of the terms on the right side of Eq. (66) are positive. However, if $\omega_e \tau_e$ and $\omega_I \tau_I$ become quite large, e.g., low ambient pressure and a fairly strong magnetic field, then U_y can be the dominant term on the right side of Eq. (66).

If some mechanism is now present to drive the ions against the electric field in the y-direction, then the direction of U_x will reverse and the cathode spot will move in the retrograde direction. A likely mechanism to cause the ions to move against the applied electric field is that of the cathode jet. When the cathode attachment region of the arc covers a very small area, then the discharge expands and accelerates the gas away from the surface. For reasonable expansion area ratios the ions can be forced to move against the field and thus initiate the retrograde motion of the arc column near the cathode. The various physical processes necessary to retrograde motion are discussed below:

1) The ions are accelerated away from the cathode spot and move against the electric field. The electromagnetic force on the ions is now in the retrograde direction. In a configuration with no forced gas flow, this ion motion is accomplished by the electromagnetic pumping force in the expanding arc column of the discharge as one moves away from the cathode attachment spot.

2) The arc current plus an added current to compensate for the ion motion is all carried by the electrons.

3) The total collision cross-section of the electrons with neutral atoms must be very much greater than the total collision cross-section for the electrons and ions. Because of this the net body force $\int j \times B \, d V$ is transferred to the neutral, non-luminous gas which is put into motion in the proper j x B direction.

4) The net force on the ions is now the resultant of the following 2 forces:

a) Electromagnetic body force in retrograde direction.

b) Body force in proper direction due to collision with electrons and atoms.

When (a) is greater than (b), the ions will move in the retrograde direction. Due to the negligible inertia of the electrons, the ion motion determines the motion of the arc column. Hence the criterion for retrograde motion of the cathode spot is that the electromagnetic forces on the ions be greater than the collision forces on them when the ions move against the applied electric field.

5.2 Retrograde Motion Experiment

Investigation of the retrograde motion phenomenon in an arc required a high level of sophistication in the design of apparatus and instrumentation. Large values of rotational velocity, small electromagnetic interaction forces, small internal clearances, and the requirement for annular cathode and anode geometries are among the problems that must be considered, many of which are more severe than "conventional" arc jet design problems.

The equipment built for these experiments had the potential to enable accurate control, measurements, and observation of the retrograde motion. However, many practical difficulties were encountered which limited the amount of useful data obtained.

Some of the more important design criteria which were incorporated into the initial geometry were:

1) Provision was made to measure the total momentum transferred to the gas due to the electromagnetic forces on the gas. This would be accomplished by measuring the torque on a plate with fins that stop the rotational component of gas velocity.
2) The magnetic field was tailored to be uniform over the region of the discharge so that the electromagnetic interaction force on the gas was just I B l, where I is the total current, B is the applied magnetic field, and l is the length of the discharge. Provision was made to vary the magnetic field B from 1,000 to over 10,000 gauss, the current I from 1 ampere to over 100 amperes, and the electrode separation l from about 2 mm to over 10 mm.
3) A comparison of the measured momentum change of the gas and the electromagnetic body force, which would give some indication of the momentum lost by viscous drag effects on the gas flow over the electrodes, was provided for.

4) The inner and outer rings that confine the discharge were electrically insulated from each other so that the potential difference parallel to the applied magnetic field developed in the discharge could be measured. This measurement would be very important in helping to determine the total electric field strength in the cathode attachment region.

The resulting device is shown schematically in Fig. 19 and in fabrication in Figs. 20 and 21. The apparatus as shown in Fig. 19 consists essentially of toroidal electrodes 6 inches in diameter. A magnetic field is focused by high-permeability iron in a radial direction between the electrodes such that an arc struck between the electrodes in a direction parallel to the axis of the electrodes will be perpendicular to the direction of the magnetic field. The cross-section of the cathode torus is conical so that the surface of the cathode to which the arc attaches is a circular line. The thin edge of the cathode was fabricated from thoriated tungsten rod formed in a circle and brazed to a copper ring. The cathode is located between two buffer rings which form an annular gas inlet nozzle at the arc attachment region of the cathode. The anode is a water cooled copper ring with a flat surface in the region of arc attachment. After the gas passes from the annular nozzle into the arc region, it must then pass through radial holes in the torque-sensing stator before discharging into the vacuum system. This stator is in close proximity to the anode and buffer rings but is suspended only at the torque sensor and does not make contact at any other region. The stator directs the gas in a radial direction such that the J x B forces added to the gas in the arc chamber are ultimately applied to the stator and measured by the torque sensor. After leaving the stator, the gas enters a large volume stilling space between the stator and the housing and then passes through an annular space between the throttle plate and the stator. The flow through the throttle plate is normally sonic; thus, the annular area can be selected to establish the internal operating pressure. Also, it was possible to bleed gas into the space upstream of the throttle plate to control the internal pressure.

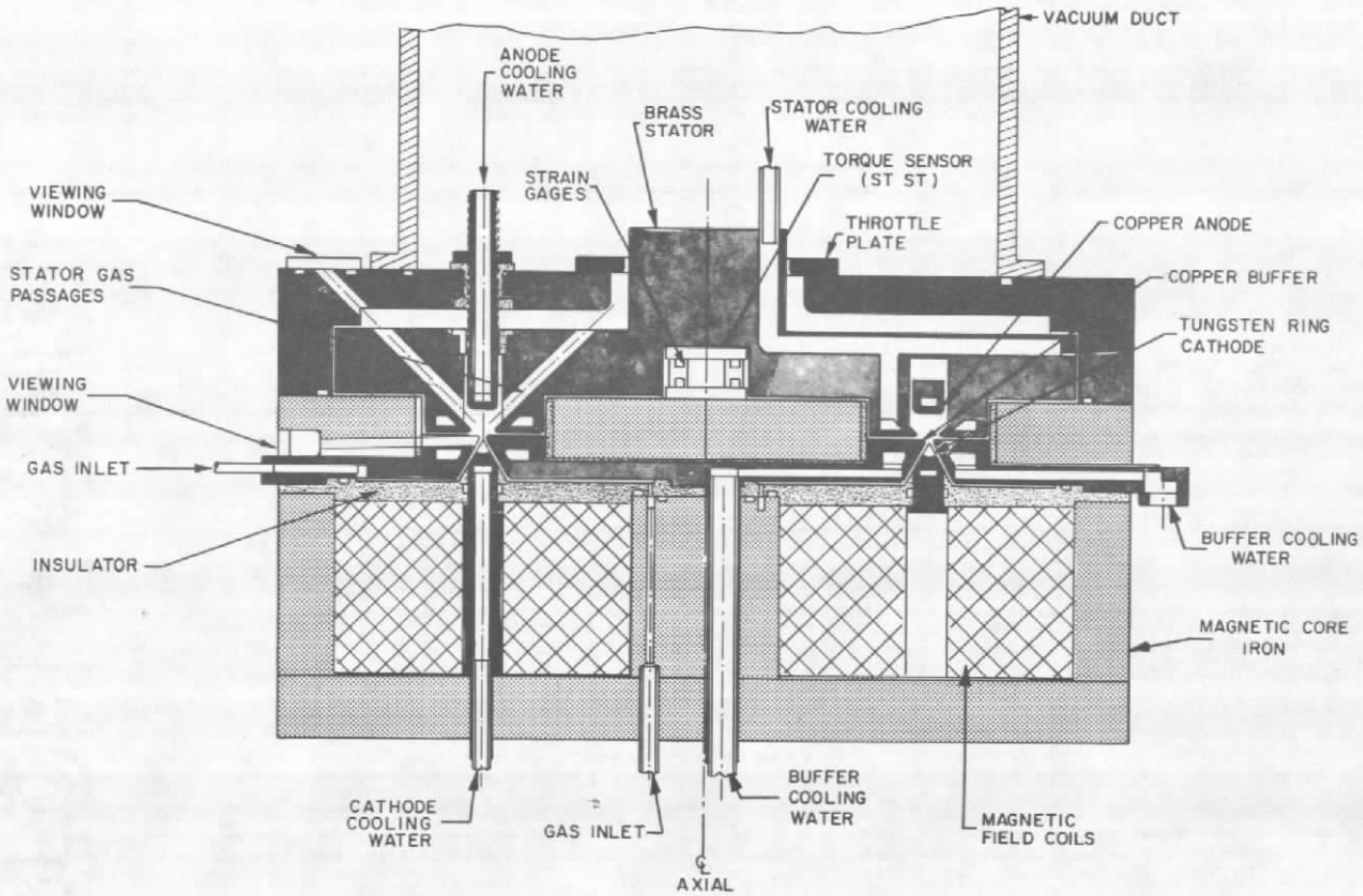

FIG. 19 RETROGRADE MOTION EXPERIMENTAL APPARATUS

FIG. 20 RETROGRADE MOTION APPARATUS MAGNETIC CIRCUIT COMPONENTS (Disassembled)

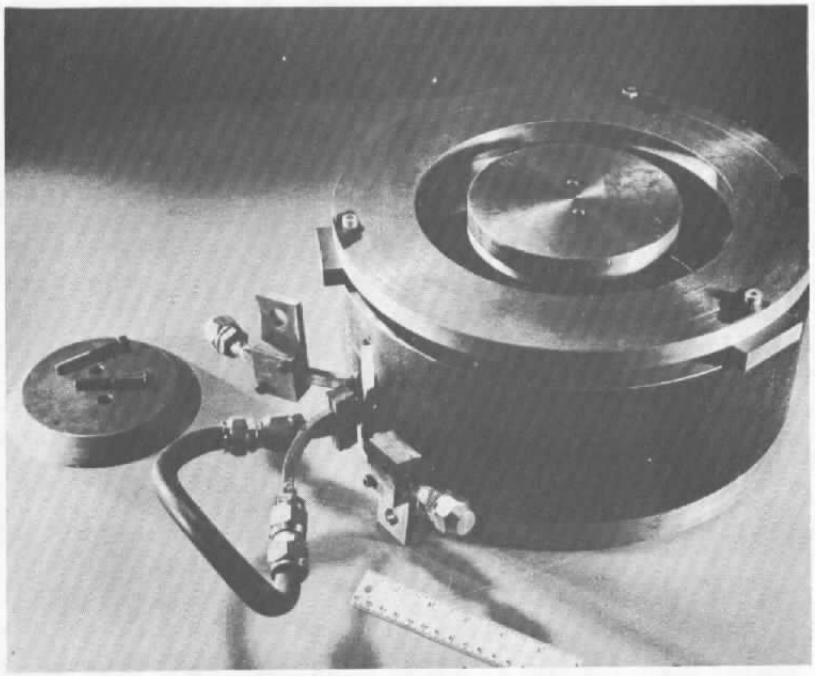

FIG. 21 RETROGRADE MOTION APPARATUS MAGNETIC CIRCUIT COMPONENTS (Assembled)

The initial series of tests were conducted with the assembly mounted in a vacuum chamber. Argon was fed into the chamber and the gas pressure was maintained between 0.5 and 15 mm. An arc was initiated between the electrodes and rotated rapidly around the ring in the J x B direction. However, it was not possible to sustain the discharge at current levels below 50 amperes, possibly because of the characteristics of the power supplies, and hence a great deal of gas heating occurred. The residual ionization level of this heated gas appeared to be high enough so that numerous attachment points appeared on the electrodes. This made it impossible to measure a rotation rate with the photocells. The pressure in the chamber was changed over quite a wide range (0.5 to 15 mm) in an effort to try and obtain a single attachment point on each electrode. This appeared to have no noticeable effect, other than causing a change in the frequency of the noise heard coming from the equipment.

As a result of the problems encountered during this test series, the equipment was modified to enable control of lower current levels ($\sim$ 1 amp) and to inject gas over the cathode tip in an attempt to stabilize a single cathode attachment point.

In the second test series, three techniques for measuring the rotation rate of the cathode spot were installed in the retrograde experiment. The photocells were used again, but this time they were mounted six inches away from the cathode, so that noise from the arc and the magnet coils was reduced. Effort was also made to electrically shield the leads completely. As a second way to measure the rotation rate, a small pick-up coil was mounted in the cathode to measure the flux change as the current density passed through it during the rotation cycle. This technique proved very reliable during experiments at the California Institute of Technology in measuring arc rotation rates. Thirdly, high speed photography (5,000 - 7,000 frames/sec.) was used to try and get the rotation rate. This technique had previously been successfully used by Mr. Eric Soehngen at ARL.

The modifications to the retrograde equipment over that used previously are shown in Fig. 22. Essentially, the cathode was buffered

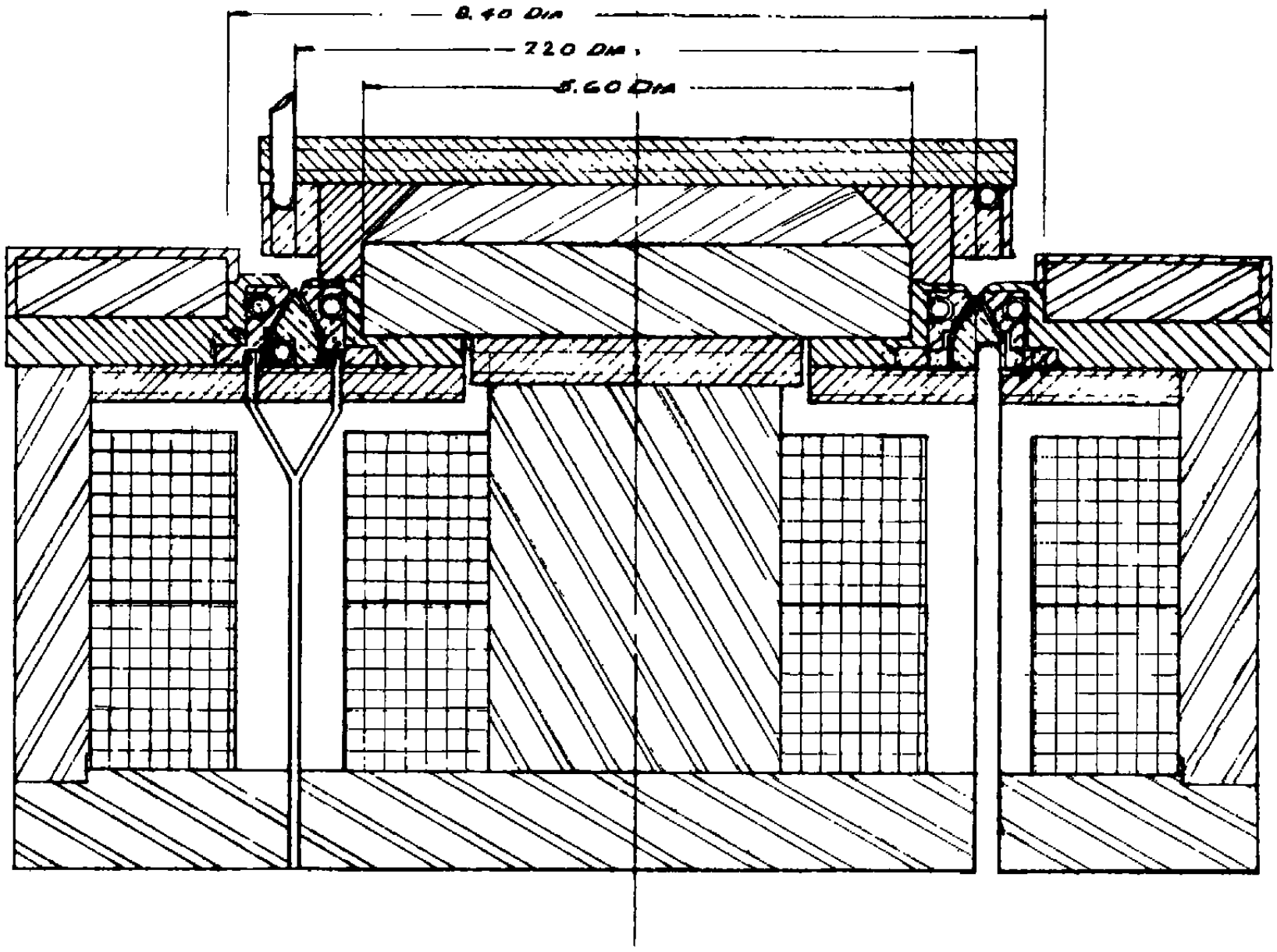

FIG. 22 MAGNETIC CIRCUIT RETROGRADE MOTION APPARATUS - PHASE I

in an attempt to force discharge attachment to the ridge. Provision was also made to flow gas over the cathode through the buffering rings.

After the retrograde equipment was fitted with buffer electrodes to confine the flow over the cathode ring, the apparatus was mounted in the vacuum chamber and connected for testing. A current of from 1 to 10 amps was passed through the discharge. The current in the magnet circuit was varied over a range of 0 to 1,000 amps. During all of the tests it was found that the current would jump intermittently to the buffers from the cathode and then to the anode. This made it impossible to measure the rotation rate of the cathode spot. The arc was observed to rotate in a rather discontinuous manner. Injecting gas between the cathode and the buffers appeared to have a significant effect on the rotation rate. However, because of the shorting to the buffer, no quantitative data could be obtained.

The equipment was then modified by adding some insulators for the buffer so that arcing to the buffers should not occur. Insulation was placed over all exposed portions of the buffers and electrodes except for the anode face and the cathode edge. This was done in an effort to prevent secondary discharges or shorting to the buffers. Numerous attempts were made to initiate the arc and measure its rotation rate. In all of these attempts the discharge burned through the insulation and attached at a point, rather than rotating around the cathode ring. Upon making a detailed examination of the configuration it was discovered that the anode had been separated from the cathode by an added 0.10" in order to mount the insulation. This made a 0.20" gap between the cathode and anode, which possibly accounted for the difficulty in obtaining a proper rotating discharge.

The gap was then reduced to 0.040" and the retrograde equipment was run several times. In no case was it found possible to stabilize the arc and obtain a significant rotation rate. The discharge was observed to move in the retrograde direction as the ambient pressure and magnetic field strength were varied. However, no consistent or reproducible rotation rates were recorded. Upon examination of the

equipment, it was found that the cathode and buffer rings had shorted together so that the discharge occurred between the buffer and the anode.

Although time consuming, the various operational problems incurred in the apparatus during this program were characteristic of the type of small practical problems arising when a new design concept is used. Although many features of the design can be improved upon, the essential design criteria are met in the device. Therefore, a future investigation should probably modify the existing apparatus where necessary rather than attempting a completely new approach.

6. CONCLUSIONS

1. A set of mechanisms have been postulated to describe the phenomena occurring at the cathodes of high current, high pressure arcs. Using these mechanisms, an analysis of the mass and energy transfer characteristics of the cathode attachment zone has been carried out and closed form solutions obtained in terms of known physical constants.

2. The predicted value of power loss to the cathode, as determined by theory, is compared to the measured values of cathode power absorption and the correlation appears to be reasonably satisfactory.

3. The theory predicts a rather strong dependence of the cathode behavior upon the pressure of the ambient gas. The details of this dependence have not yet been thoroughly investigated.

4. The theory introduces the electrode configuration into the predicted performance capability of the cathode. This should eventually let us optimize the cathode shape for any desired performance.

5. A critical condition for the arc attachment to a cathode of conical configuration has been found. An unconfined arc will not attach to the cone tip when the ambient pressure is lower than some critical value. A diffuse attachment to the side of the cone occurs at the lower pressures. The "critical" pressure at which this phenomena occurs appears to be approximately the same, independent of whether the gas pressure is increased or decreased through the critical value.

6. A self-consistent explanation for the phenomenon known as "retrograde motion" is postulated. Preliminary expressions are derived for the retrograde velocity of the cathode spot in terms of the magnetic field strength, gas properties, and the velocity of the gas in the direction of the applied electric field.

7. RECOMMENDATIONS

1. Spectroscopic measurements should be made of the cathode attachment zone to attempt to detect all species present there. In particular, efforts should be made to determine whether or not atoms and ions of cathode material exist away from the surface. If they are found, then the distance that they extend away from the surface should be determined.

2. Measurements should be made of the power loss, material loss rate, and area of arc attachment on cathode surfaces of various configurations over a wide range of arc current and ambient gas pressure.

3. The phenomenon of a "critical" pressure (noted in Section 6.5 of Conclusions) for the arc attachment to a conical cathode tip should be investigated experimentally, in detail.

4. The analysis of the cathode attachment region should be extended to include the effects of the radiation from the gas to the cathode surface and of the radiation from the cathode.

5. The analysis should next be modified so that it can predict the loss rate of cathode material.

6. The energy equation for the electrons should be evaluated so that non-equilibrium electron temperature effects can be introduced into the various cathode mechanisms.

7. The analysis should be applied to the anode attachment zone of high current, high pressure discharges.

REFERENCES

1. Ecker, G., "Electrode Components of the Arc Discharge", Ergeb. exakt. Naturwiss 33, 1-104 (1961)

2. Cann, Teem, Buhler and Bronson, "Magnetogasdynamic Accelerator Techniques", AEDC-TDR-62-145 (1962)

3. Cann, G.L., et al "Thermal Arc Jet Research", Aeronautical Systems Division, Technical Documentary Report No. ASD-TDR-63-632, Classified Confidential (Title Unclassifed), Electro-Optical Systems, Inc., (15 August 1963)

4. Handbook of Thermophysical Properties of Solid Materials. The Macmillan Co. (1961) (Sponsored by WADD)

5. Handbook of Chemistry and Physics. Chemical Rubber Publishing Co. (1947)

6. Lee, T. H., "T-F Theory of Electron Emission in High-Current Arcs", J. Appl. Phys. 30, 166 (1959).

7. Bade, William, et al, "Theoretical and Experimental Investigation of Arc Plasma Generation Technology" Aeronautical Systems Division, Technical Documentary Report No. ASD-TDR-62-729, Part II, Vol. 1, AVCO Corporation, September 1963.

8. Neuroth, P. W. and Gibbs, T. W., "Arc Cathode Emission Mechanisms at High Currents and Pressures", J. Appl. Phys. 34, 277 (1913).